Copy
RM L54K15

NACA RM L54K15

NACA

RESEARCH MEMORANDUM

AERODYNAMIC LOADING CHARACTERISTICS IN SIDESLIP OF A 45° SWEPTBACK WING WITH AND WITHOUT A FENCE AT HIGH SUBSONIC SPEEDS

By Richard E. Kuhn and Andrew L. Byrnes, Jr.

Langley Aeronautical Laboratory
Langley Field, Va.

NATIONAL ADVISORY COMMITTEE
FOR AERONAUTICS

WASHINGTON
January 28, 1955

NATIONAL ADVISORY COMMITTEE FOR AERONAUTICS

RESEARCH MEMORANDUM

AERODYNAMIC LOADING CHARACTERISTICS IN SIDESLIP OF A 45° SWEPTBACK WING WITH AND WITHOUT A FENCE AT HIGH SUBSONIC SPEEDS

By Richard E. Kuhn and Andrew L. Byrnes, Jr.

SUMMARY

An investigation of the effects of sideslip on the aerodynamic loading characteristics of a 45° sweptback wing of aspect ratio 4 has been conducted in the Langley high-speed 7- by 10-foot tunnel. The investigation included the effects of fences and covered a range of angle of attack and angle of sideslip at Mach numbers from 0.7 to 0.95.

The results indicate, as would be expected, that at low angles of attack the root bending moment increases with sideslip on the leading wing and decreases with sideslip on the trailing wing. However, at a Mach number of 0.70 and at angles of attack of 12° to 17° with the fence off, the root bending moment on the trailing wing exceeded that on the leading wing at all angles of sideslip. In general (except near an angle of attack of 12°), the lateral center of pressure did not vary much with angle of sideslip. The variations of root bending moment and of the coefficient of rolling moment due to sideslip are due primarily to variation in normal-force coefficient on the leading and trailing wings rather than to shifts in the lateral centers of pressure. With the fence installed, the root bending moment of the leading wing was always greater than that of the trailing wing, and the coefficient of rolling moment due to sideslip remained negative throughout the angle-of-attack range.

INTRODUCTION

Investigations of the rolling moment due to sideslip of swept wings (refs. 1 and 2, for example) have shown that at the higher angles of attack the rolling moment due to sideslip sometimes varies erratically with lift coefficient. Accordingly, in order to obtain some data that may help to provide a better understanding of the reasons for these variations, and also to provide information on loads due to sideslip, an investigation of

the distribution of pressure on a 45° sweptback wing of aspect ratio 4 in combination with a fuselage was undertaken.

The erratic variations of rolling moment due to sideslip for sweptback wings are usually attributed to the effects of tip stalling. Wing fences are known to be effective in delaying tip stalling to higher angles of attack; therefore, the effects of a fence installed at the 65-percent-semispan station were also investigated.

This paper presents the load distribution at angles of sideslip of approximately 0°, 4°, 8°, and 12° for the clean wing and for the wing with a fence installed at the 65-percent-semispan station. The investigation covered an angle-of-attack range from 4° to 24° and a Mach number range from 0.70 to 0.95. The load distributions through the angle-of-attack range at zero angle of sideslip have been presented already in reference 3, and the effect of steady rolling on the load distribution on the wing is shown in reference 4. The aerodynamic-force characteristics of this configuration in sideslip and pitch are presented in references 2 and 5, respectively. Some of the data from the present investigation have been summarized briefly in reference 6.

COEFFICIENTS AND SYMBOLS

M	Mach number
R	Reynolds number
P	pressure coefficient, $\frac{P_l - P_o}{q}$ or $\frac{P_u - P_o}{q}$
p	local static pressure, lb/sq ft
p_o	free-stream static pressure, lb/sq ft
q	dynamic pressure, $\frac{1}{2}\rho V^2$, lb/sq ft
ρ	air density, slugs/cu ft
V	free-stream velocity, fps
c	local wing chord, ft
c_{av}	average wing chord, S/b, ft

b	wing span, ft
b_e	exposed span, $b - D$, ft
S	wing area, sq ft
D	maximum fuselage diameter
x	chordwise distance from leading edge of local chord, ft
y	spanwise distance perpendicular to fuselage center line, ft
$\Delta\left(\frac{x}{c}\right)$	increment of local chord over which pressure at a particular orifice is assumed to act
c_n	section normal-force coefficient, $\sum_{x/c=0}^{1} (P_l - P_u)\,\Delta\left(\frac{x}{c}\right)$
c_m	section pitching moment about 0.25 local chord, $\sum_{x/c=0}^{1} (P_u - P_l)\left(\frac{x}{c} - 0.25\right)\Delta\left(\frac{x}{c}\right)$
C_{N_e}	normal-force coefficient of one exposed wing, $\frac{b}{b_e}\int_{.14}^{1.0} c_n \frac{c}{c_{av}}\, d\,\frac{y}{b/2}$
C_{B_e}	bending-moment coefficient of one exposed wing, $\left(\frac{b}{b_e}\right)^2 \int_{.14}^{1.0} c_n \frac{c}{c_{av}} \frac{y - D/2}{b/2}\, d\,\frac{y}{b/2}$
α	angle of attack, deg
β	angle of sideslip, deg
$\frac{X}{c}$	local longitudinal center of pressure, $0.25 - \frac{c_m}{c_n}$
$\frac{Y_e}{b_e/2}$	lateral center of pressure measured from fuselage surface, C_{B_e}/C_{N_e}

[redacted]

C_l rolling-moment coefficient about fuselage center line,

$$-\frac{1}{4}\int_{-1.0}^{1.0} c_n \frac{c}{c_{av}} \frac{y}{b/2} d\frac{y}{b/2}$$

$$C_{l_\beta} = \frac{\partial C_l}{\partial \beta}$$

Subscripts:

u upper surface

l lower surface

MODEL AND APPARATUS

A drawing of the wing-fuselage configuration tested is shown in figure 1. The wing had a quarter-chord sweep of 45°, an aspect ratio of 4, a taper ratio of 0.6, and an NACA 65A006 airfoil section, and was of composite construction, consisting of a steel core with a bismuth-tin covering to give the desired contour. One hundred and fifteen static-pressure orifices were located in the upper and lower surfaces of the wing and were distributed along five spanwise stations parallel to the plane of symmetry (20-, 60-, and 95-percent semispan on the right wing and 40- and 80-percent semispan on the left wing). The chordwise locations of the pressure orifices are indicated in table I. The wing was mounted on the fuselage in a midwing position with zero dihedral and zero incidence. The ordinates of the circular fuselage are given in reference 5.

The model was tested on the sting-type support system shown in figure 2. With this support system the model can be remotely operated through a 28° angle-of-attack range. Interchangeable couplings in the sting behind the model were used to set the model at angles of sideslip of 0°, 4°, 8°, and 12°.

The details of the fences used in the investigation are shown in figure 1. The brass fences were mounted on the wing at the 65-percent-semispan station so that the mounting clips did not protrude above the wing surface.

TESTS AND CORRECTIONS

The tests were conducted in the Langley high-speed 7- by 10-foot tunnel through a Mach number range from approximately 0.70 to 0.95, corresponding to a Reynolds number range from 2.7×10^6 to 3.0×10^6. The size of the model caused the tunnel to choke at a Mach number of 0.96 at zero angle of attack. The blocking corrections which were applied to the Mach number were determined by the method of reference 7.

The angle of attack and angle of sideslip have been corrected for the deflection of the sting support system.

The aeroelastic deflection characteristics of this wing (as determined from static loadings) are presented in reference 2. No aeroelastic corrections have been applied to these data.

RESULTS AND DISCUSSION

Load Distributions

The effect of sideslip on the span-load distribution is shown in figures 3 and 4. In general, at the lower angles of attack (in the range of linear variation of lift with angle of attack), the loading on the leading wing was increased because of sideslip, and the loading on the trailing wing was decreased as would be expected. At the higher angles of attack, the effects of sideslip on the loading are sometimes reversed. At these higher angles of attack the effects of sideslip probably are a function of the extent and rate of change of stalling on the wing.

The effects of sideslip on the local chordwise center of pressure (figs. 5 and 6) also vary appreciably over the surface of the wing. Increasing the sideslip angles to 12° causes local center-of-pressure movements as large as 20 percent of the local chord. In the low angle-of-attack range, there appears to be a tendency for the load to move rearward at the tip of the leading wing and forward at the tip of the trailing wing. This tendency is more pronounced at the higher Mach numbers. The rearward movement of the center of load on the leading tip probably is due to the leading tip acting somewhat like a wing leading edge. At a sideslip angle there is a component of free-stream velocity that is normal to the wing tip and the combination of this component with the tip vortex produces an additional loading on the tip. The center of this additional loading is located farther rearward than the center of the angle-of-attack-type load. This additional load combines with the

angle-of-attack load and results in a rearward movement of the center of pressure. These effects can also be seen in the chord load distributions presented in figure 7. (See parts (c) and (d) of fig. 7.)

Root Bending-Moment Coefficient

In the symmetrical flight condition (zero sideslip) the critical root-bending-moment condition is usually determined by the gross weight of the airplane, the design-load factor, and the most outward location of the center of pressure on the wing. When the airplane is in a sideslip attitude, however, there is an additional increment of root bending moment that must be considered. At low angles of attack, the root bending moment of the leading wing increases with sideslip angle (fig. 8). At these low angles of attack, the lateral center of pressure (fig. 9) does not change with sideslip angle. The increase in root bending moment is, therefore, due to an increase in normal force (fig. 10). Under these conditions, the critical bending condition would occur on the leading wing and would depend on the sideslip angle reached.

In general (except near an angle of attack of 12°), the lateral center of pressure did not change much with sideslip angle. At an angle of attack of 16.7° ($M = 0.7$, fence off), however, the normal force on the trailing wing increases with sideslip angle in contrast to the expected decrease that occurs at lower angles of attack (fig. 10). The bending moment on the trailing wing then increases at this angle of attack and the bending moment on the leading wing decreases (fig. 8). It may be possible under these conditions, then, to reach a condition of extreme sideslip where the root bending moment of the trailing wing would become the critical condition.

With the fence installed, the root bending moment of the trailing wing is always less than that of the leading wing and the critical bending condition, therefore, would always be expected to occur on the leading wing.

Rolling Moment Due to Sideslip

The force data of reference 2 indicate a nonlinear variation of the coefficient of rolling moment due to sideslip C_{l_β} with angle of attack α. The force data of reference 2 are compared in figure 11 with rolling moment due to sideslip as determined by integration of the span-load distributions presented herein. In general, the variations with angle of attack are in good agreement although the absolute magnitudes differ to some extent. Part of the disagreement in magnitude may be due to the limited number of spanwise stations from which the span-load distributions were determined.

Although there are no force test data available for substantiation, integration of the pressure-distribution data indicates that, with fences installed, the derivative C_{l_β} does not reverse sign under conditions for which reversal was noted for the clean wing.

The data of figures 11 and 12 indicate that the variations of C_{l_β} with angle of attack (except near an angle of attack of 12°), are traceable to differences in the variation of normal-force coefficient with angle of attack on the leading and trailing wing. For example, at low angles of attack, a Mach number of 0.7, and with the fence off (fig. 12(a)), the normal-force-curve slope on the leading wing is greater than the normal-force-curve slope on the trailing wing which produces the expected stable (or negative) values of C_{l_β}. As the angle of attack is increased, however, the leading wing, which has less sweep than when at zero sideslip, begins to stall earlier and levels off at a lower normal-force coefficient than when at zero sideslip. The trailing wing, on the other hand, has more sweep and experiences an increase in normal-force-curve slope at about 6°. At higher angles of attack (13° to 17°), where the normal-force coefficient on the leading wing has leveled off, the trailing-wing normal-force coefficient still is increasing and reaches higher values than on the leading wing. This crossover of the normal-force curves results in the reversal of sign of C_{l_β} in this angle-of-attack range (fig. 11).

At the higher Mach number and with the fence installed, the normal-force curves do not cross and the coefficient of rolling moment due to sideslip C_{l_β} remains negative.

CONCLUSIONS

An investigation of the effects of sideslip on the aerodynamic loading characteristics of a 45° sweptback wing indicates the following conclusions:

1. At low angles of attack the root bending moment increases with sideslip on the leading wing and decreases on the trailing wing as would be expected. At a Mach number of 0.7 and at angles of attack of 12° to 17° with the fence off, however, the root bending moment on the trailing wing exceeded that on the leading wing.

2. In general (except near an angle of attack of 12°), the lateral center of pressure does not change much with sideslip. The variations in root bending moment and in the coefficient of rolling moment due to sideslip

C_{l_β} are due primarily to variations in normal-force coefficients on the leading and trailing wings rather than to lateral center-of-pressure travel.

3. With the fence installed, the root bending moment of the leading wing was always greater than that of the trailing wing and the coefficient of rolling moment due to sideslip remains negative throughout the angle-of-attack range.

Langley Aeronautical Laboratory,
National Advisory Committee for Aeronautics,
Langley Field, Va., November 5, 1954.

REFERENCES

1. Malvestuto, Frank S., and Kuhn, Richard E.: Examination of Recent Lateral-Stability-Derivative Data. NACA RM L53I08a, 1953.

2. Kuhn, Richard E., and Fournier, Paul G.: Wind-Tunnel Investigation of the Static Lateral Stability Characteristics of Wing-Fuselage Combinations at High Subsonic Speeds – Sweep Series. NACA RM L52G11a, 1952.

3. Kuhn, Richard E., Wiggins, James W., and Byrnes, Andrew L., Jr.: Wind-Tunnel Investigation of the Effects of a Fence and a Leading-Edge Notch on the Aerodynamic Loading Characteristics in Pitch of a 45° Sweptback Wing at High Subsonic Speeds. NACA RM L53H24, 1953.

4. Wiggins, James W., and Kuhn, Richard E.: Wind-Tunnel Investigation of the Effects of Steady Rolling on the Aerodynamic Loading Characteristics of a 45° Sweptback Wing at High Subsonic Speeds. NACA RM L53J01a, 1953.

5. Kuhn, Richard E., and Wiggins, James W.: Wind-Tunnel Investigation of the Aerodynamic Characteristics in Pitch of Wing-Fuselage Combinations at High Subsonic Speeds. Aspect-Ratio Series. NACA RM L52A29, 1952.

6. Williams, Claude V., and Kuhn, Richard E.: A Study of the Aerodynamic Loads on Sweptback Wings at Transonic Speeds. NACA RM L53E08b, 1953.

7. Hensel, Rudolph W.: Rectangular-Wind-Tunnel Blocking Corrections Using the Velocity-Ratio Method. NACA TN 2372, 1951.

TABLE I.- PRESSURE-ORIFICE STATIONS

[Distribution of orifices same for all spanwise stations]

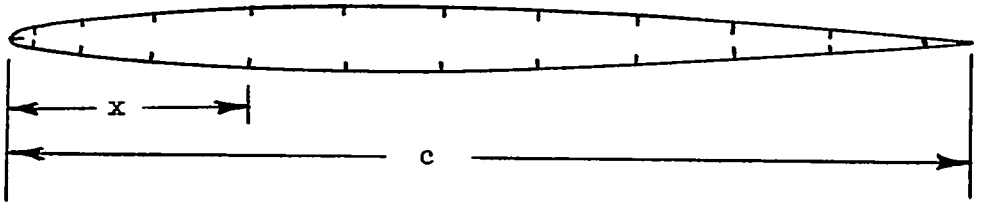

Upper	Lower
x/c	x/c
0	0
.025	.025
.075	.075
.150	.150
.250	.250
.350	.350
.450	.450
.550	.550
.650	.650
.750	.750
.850	.850
.950	.950

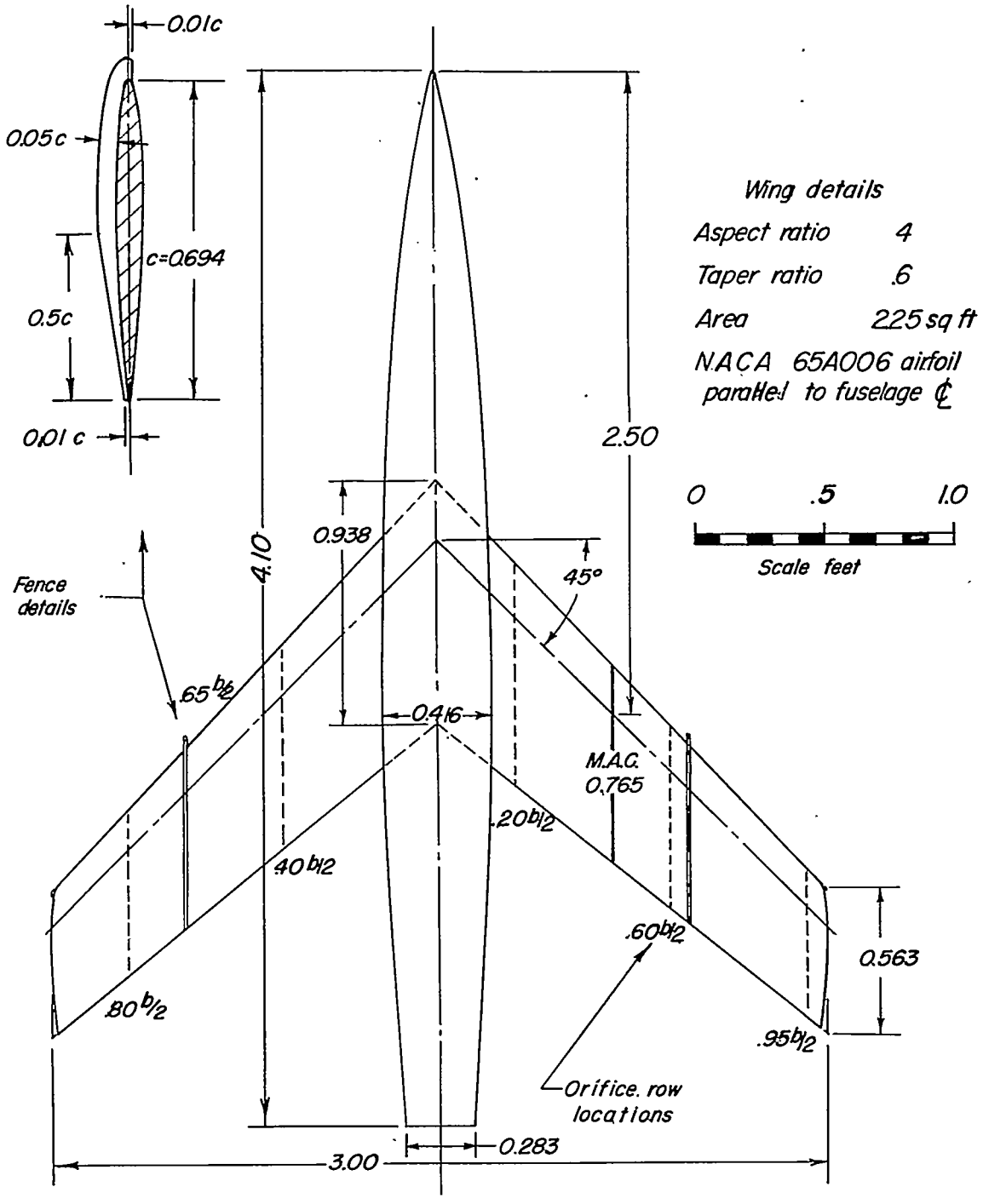

Figure 1.- Drawing of the model. All dimensions are in feet.

[redacted]

L-72400

Figure 2.- Photograph of model installed on variable angle-of-attack sting. $\beta = -4^{\circ}$.

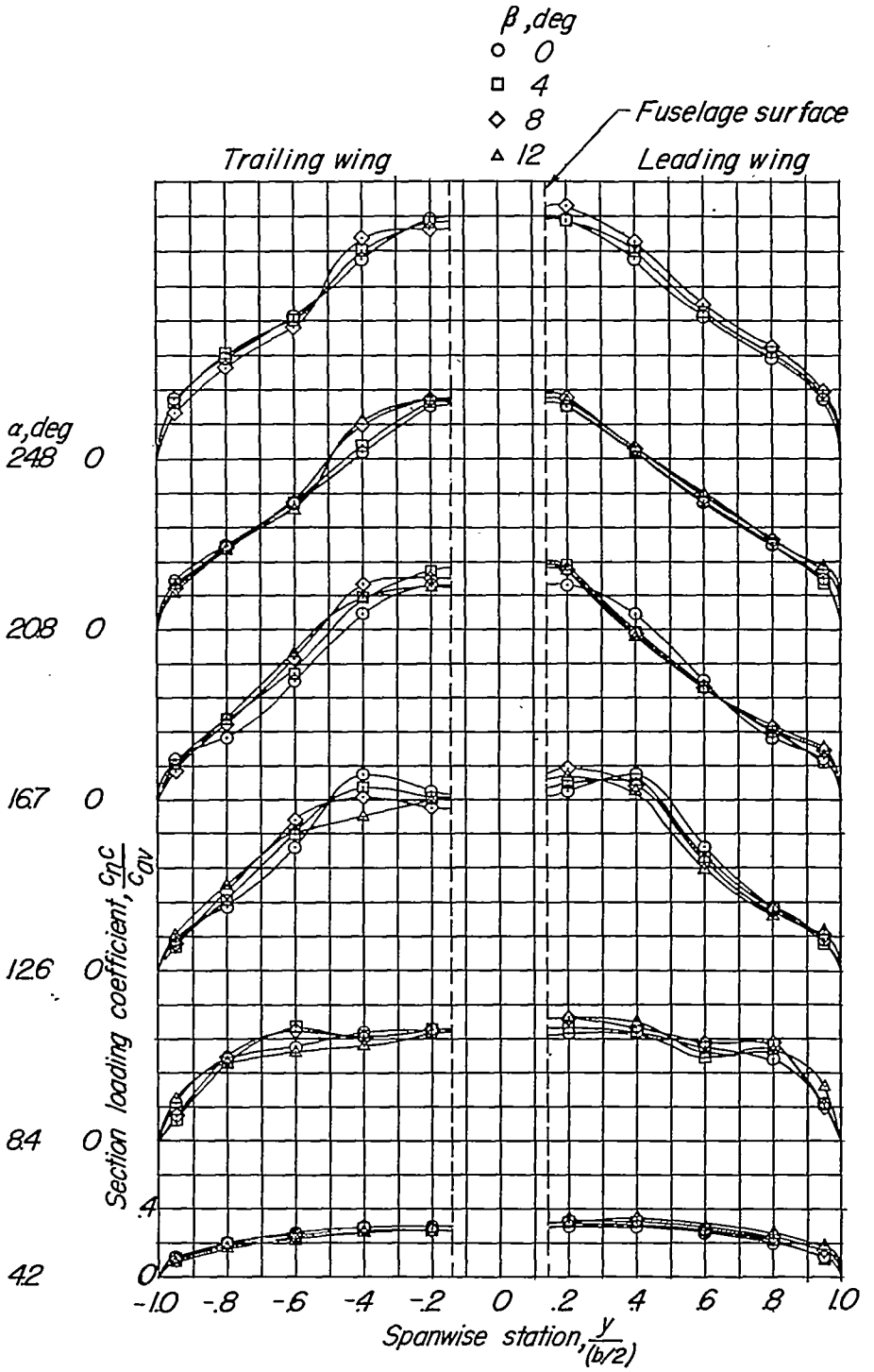

(a) M = 0.70; fence off.

Figure 3.- Effect of sideslip on span-load distribution with fence off.

[redacted]

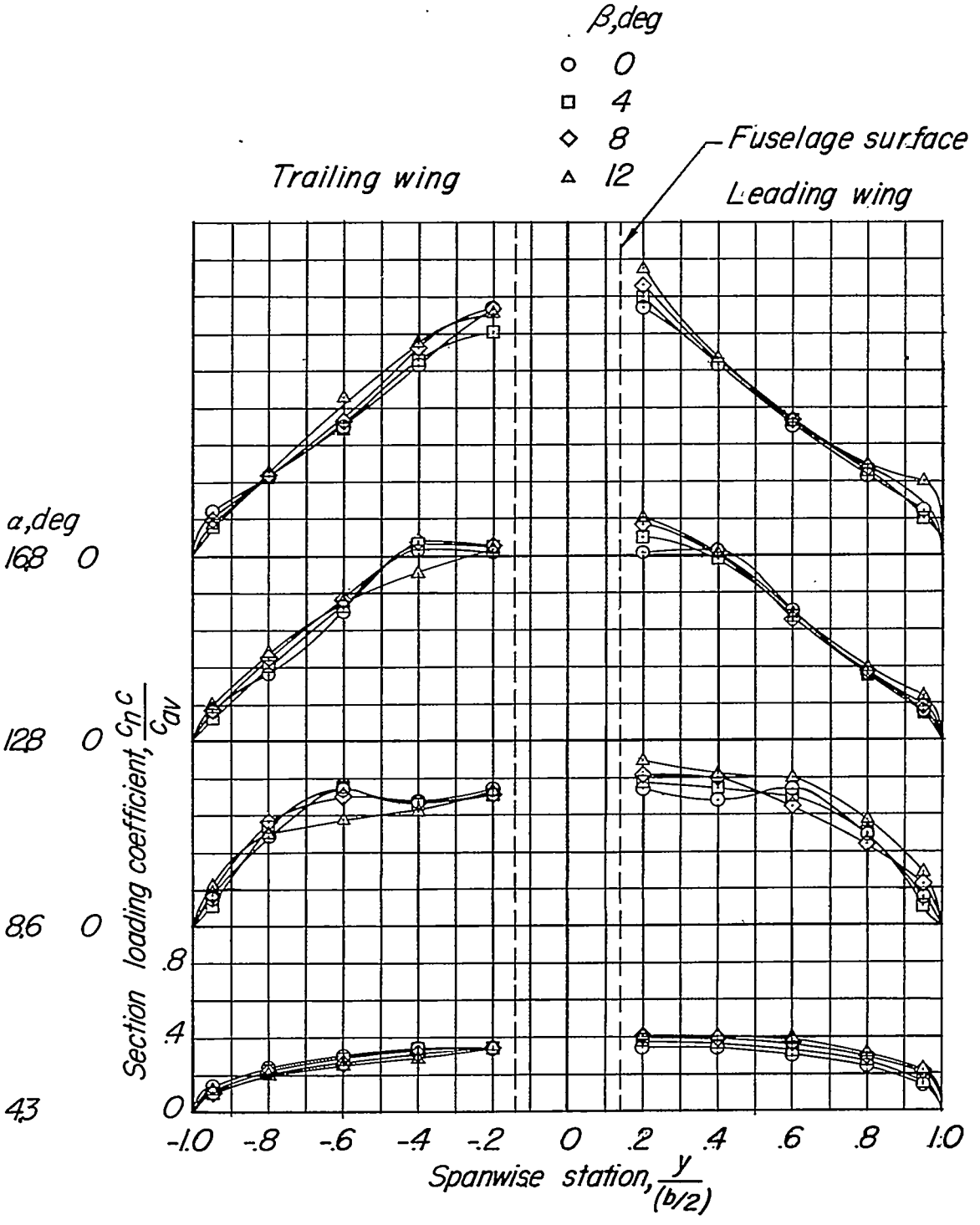

(b) M = 0.85; fence off.

Figure 3.- Continued.

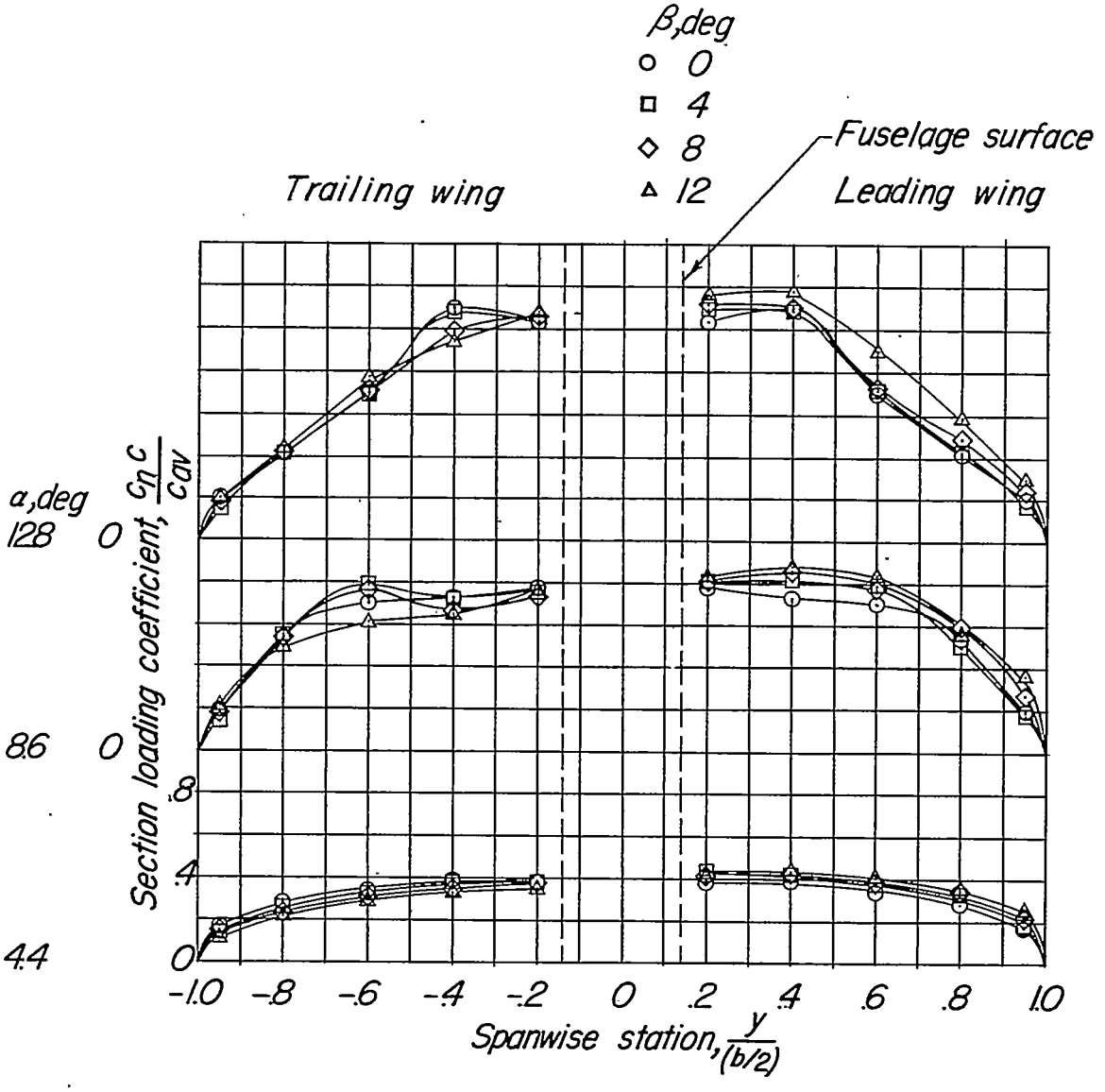

(c) M = 0.91; fence off.

Figure 3.- Continued.

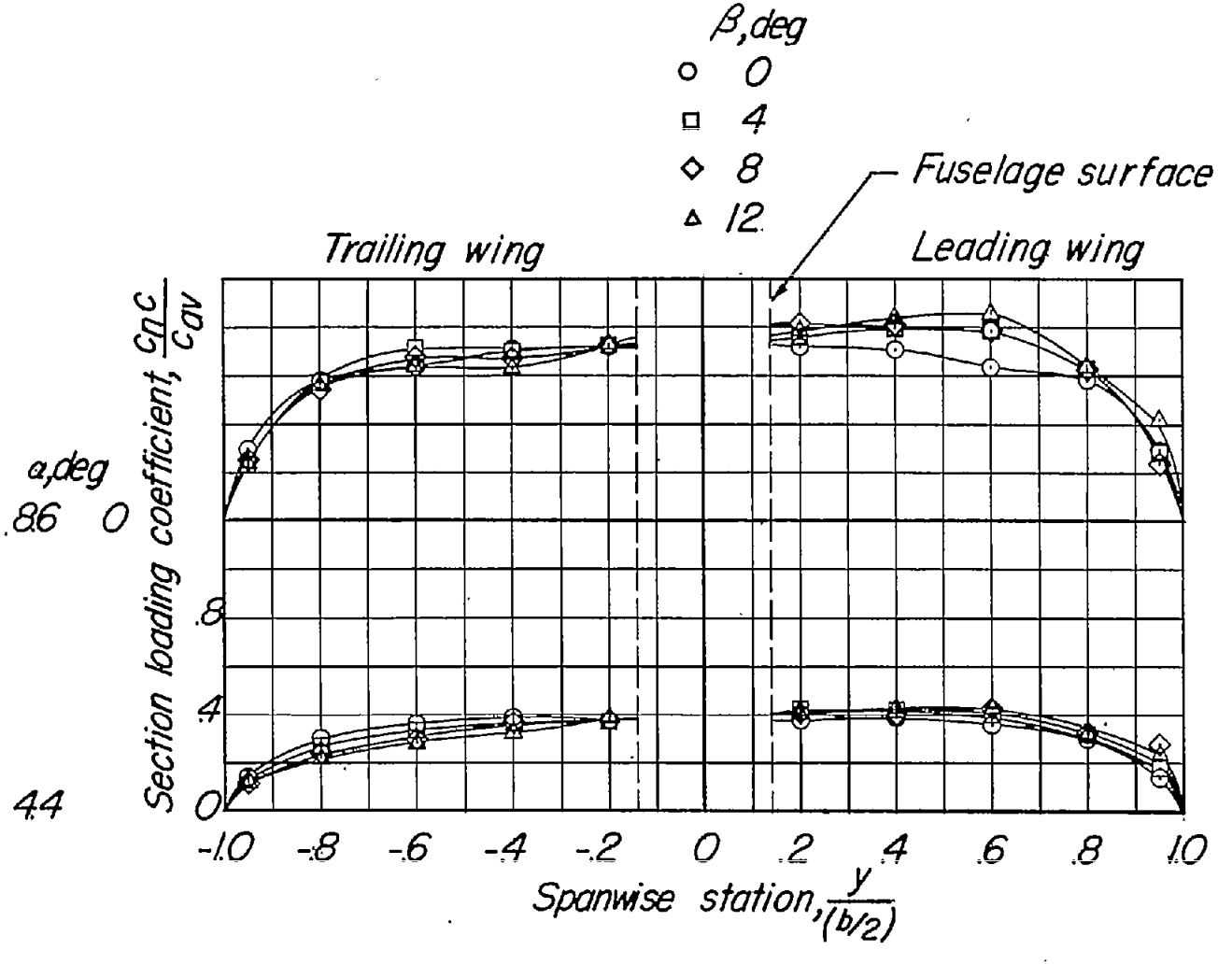

(d) M = 0.93; fence off.

Figure 3.- Continued.

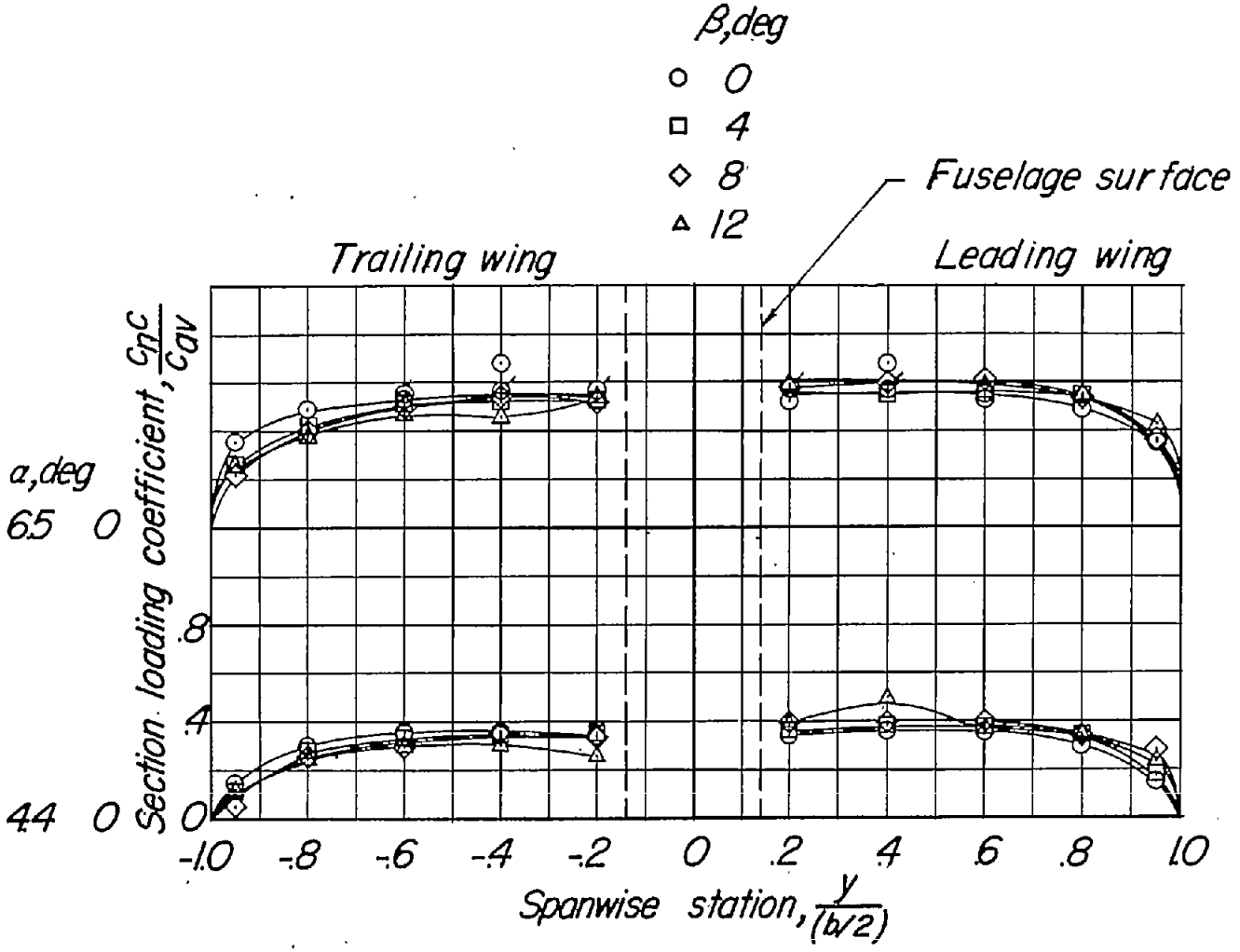

(e) M = 0.95; fence off.

Figure 3.- Concluded.

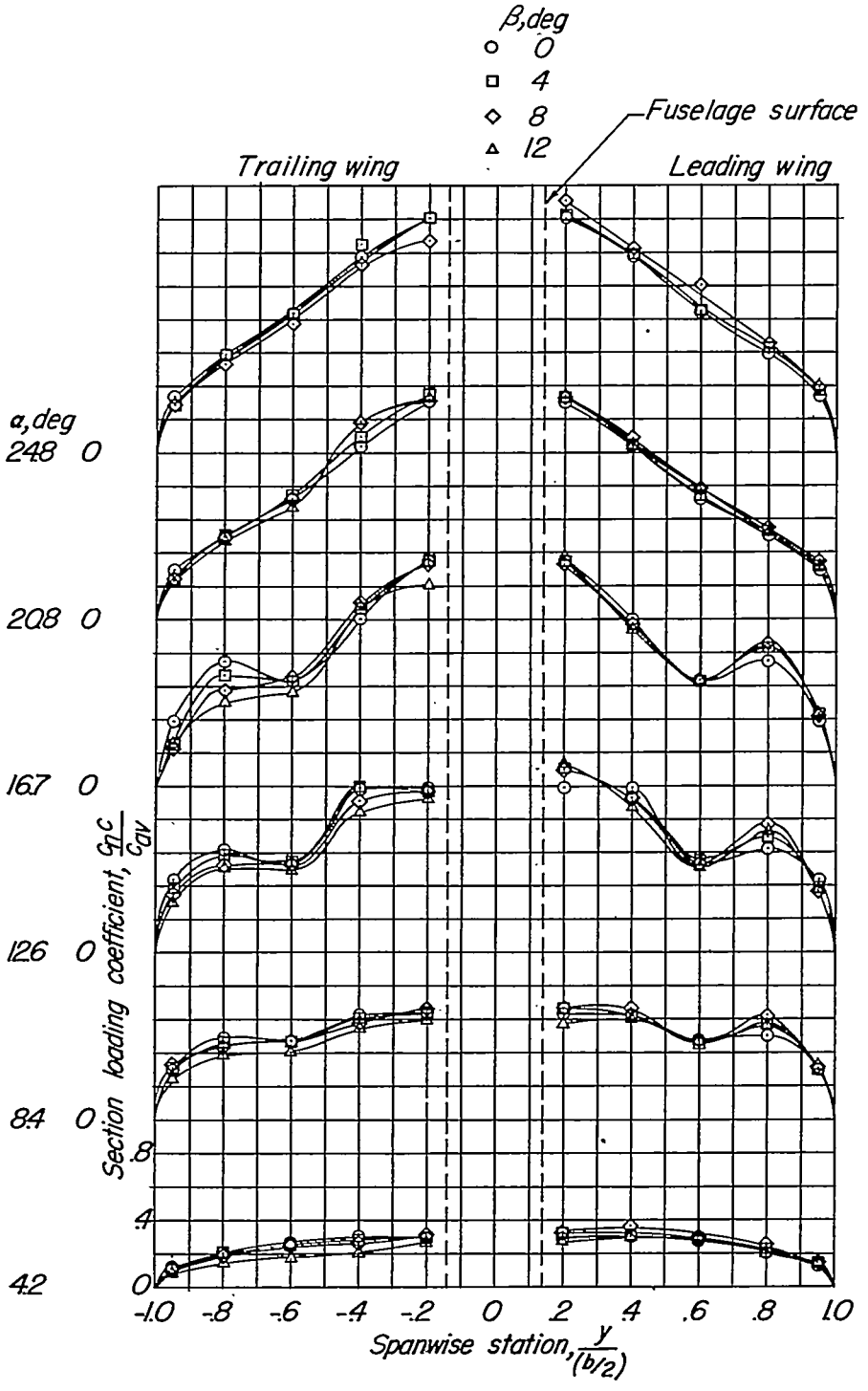

(a) M = 0.70; fence on.

Figure 4.- Effect of sideslip on span-load distribution with fence on.

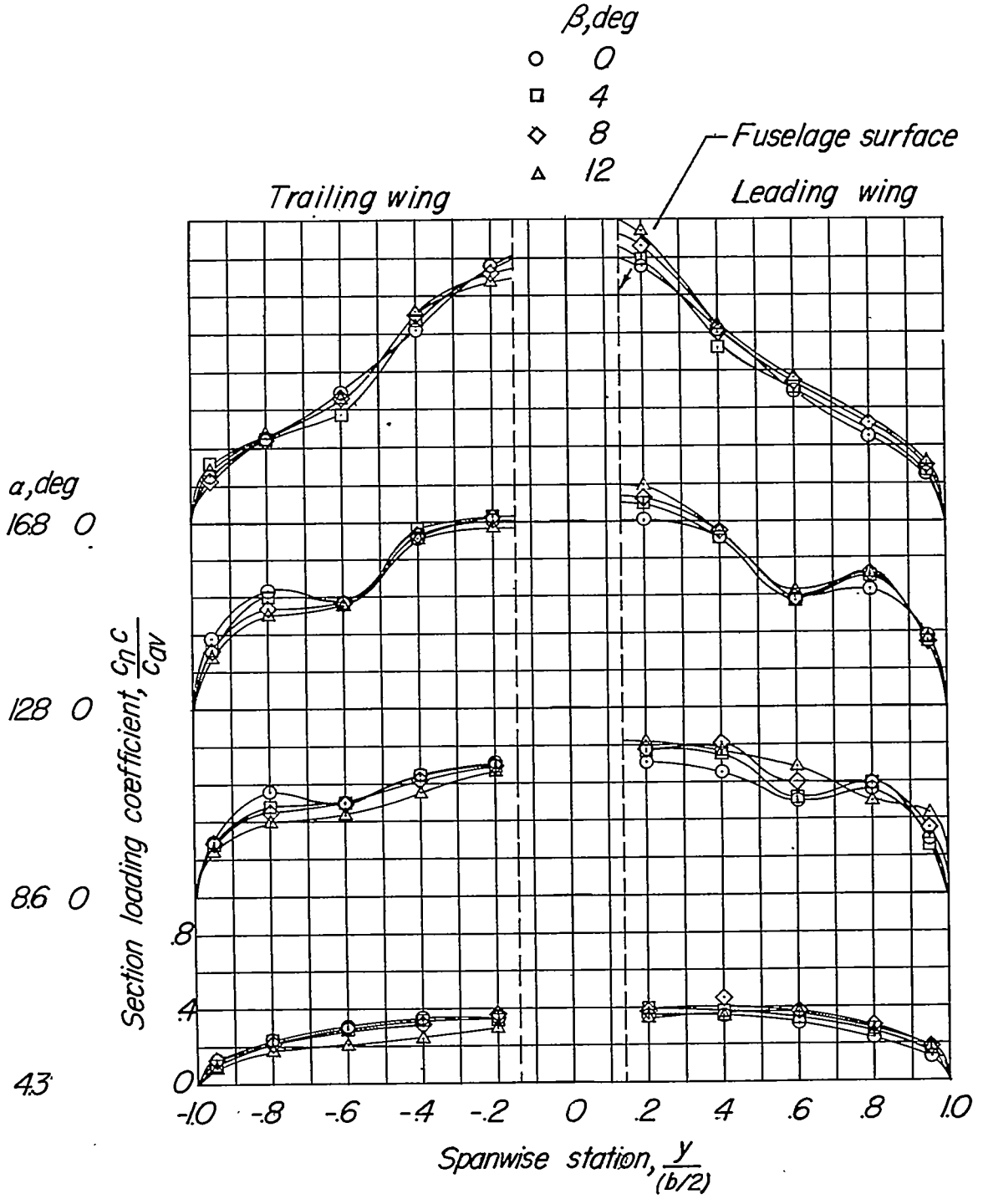

(b) M = 0.85; fence on.

Figure 4.- Continued.

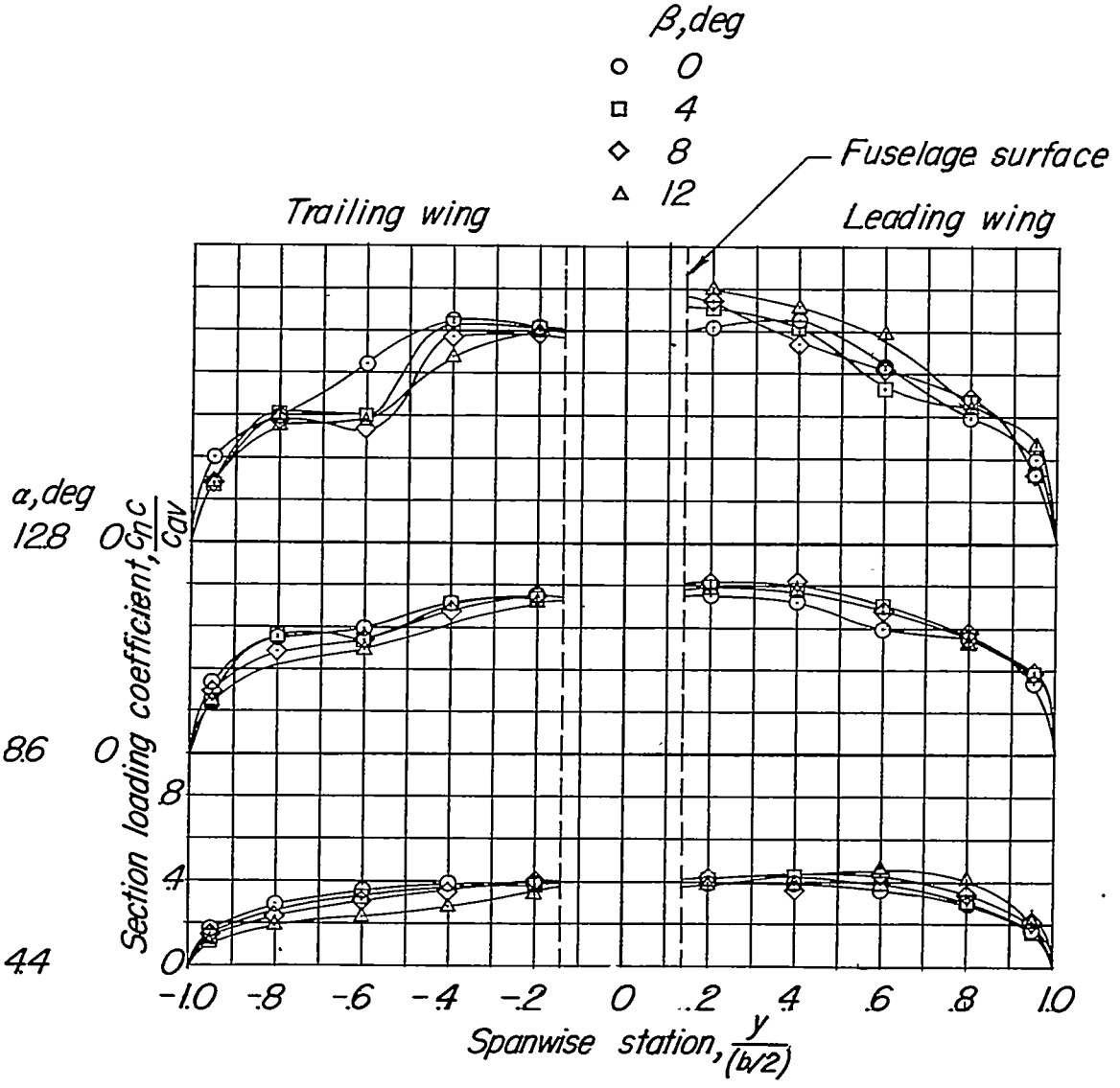

(c) M = 0.91; fence on.

Figure 4.- Continued.

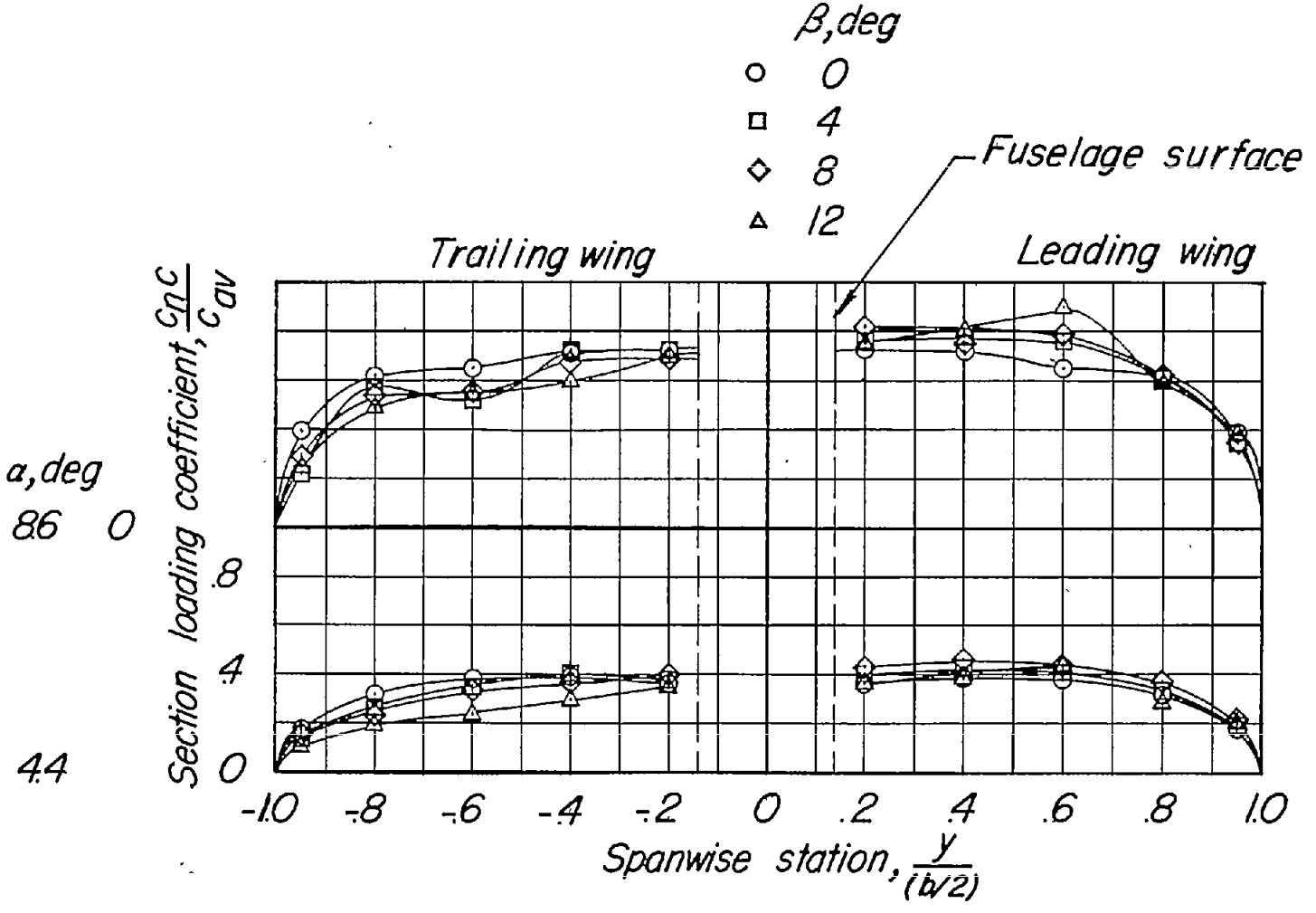

(d) M = 0.93; fence on.

Figure 4.- Continued.

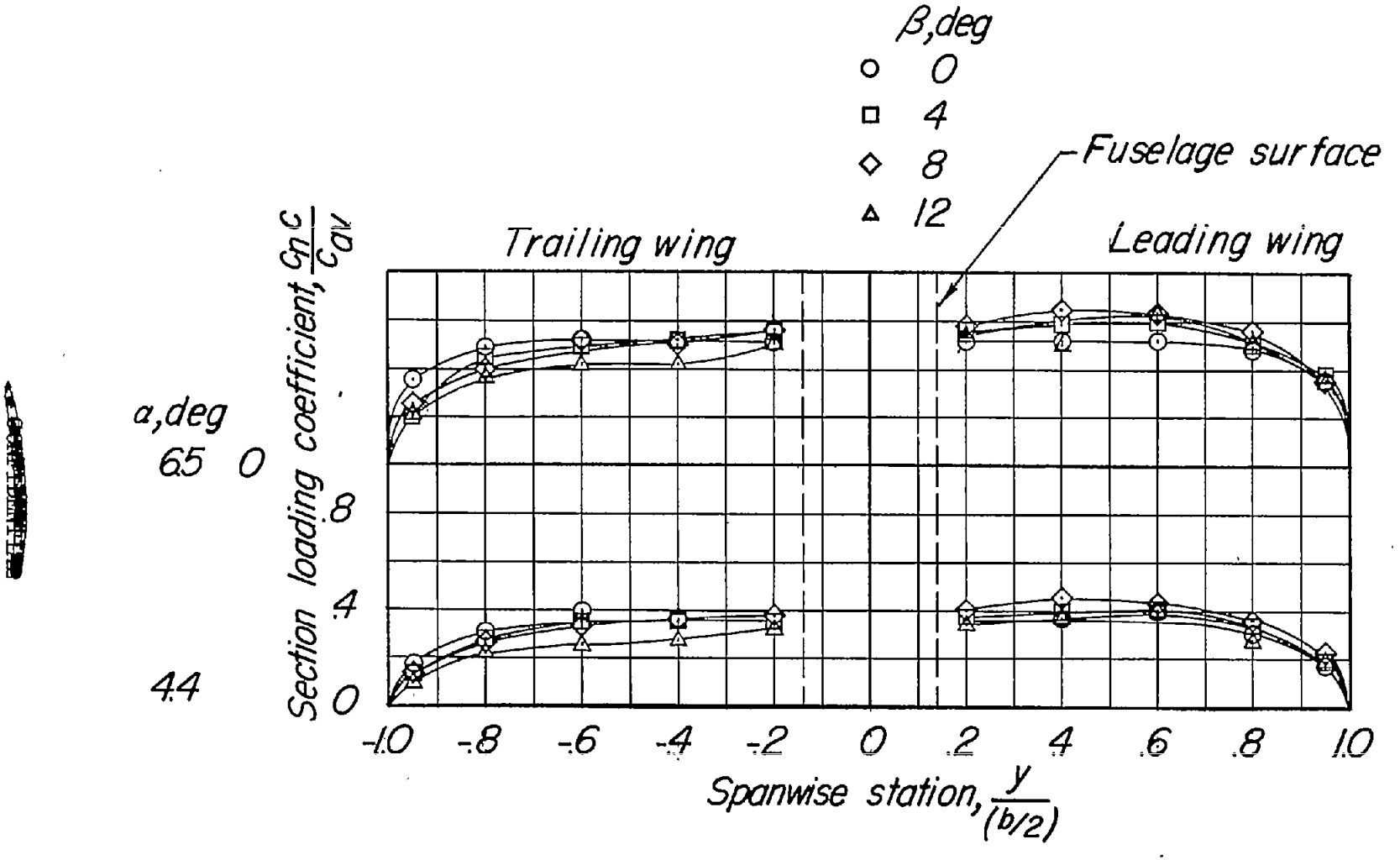

(e) M = 0.95; fence on.

Figure 4.- Concluded.

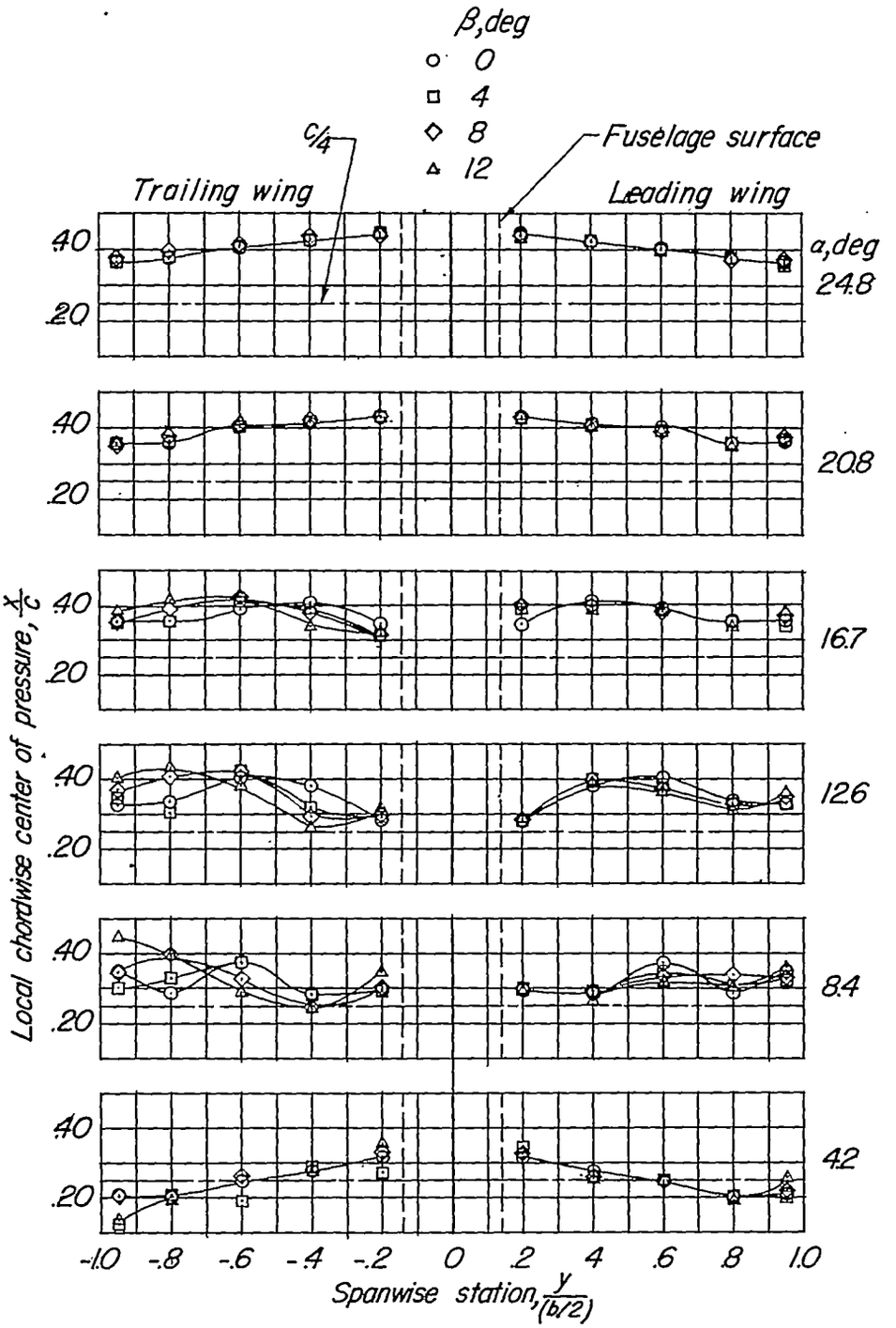

(a) M = 0.70; fence off.

Figure 5.- Effect of sideslip on location of local chordwise center of pressure with fence on.

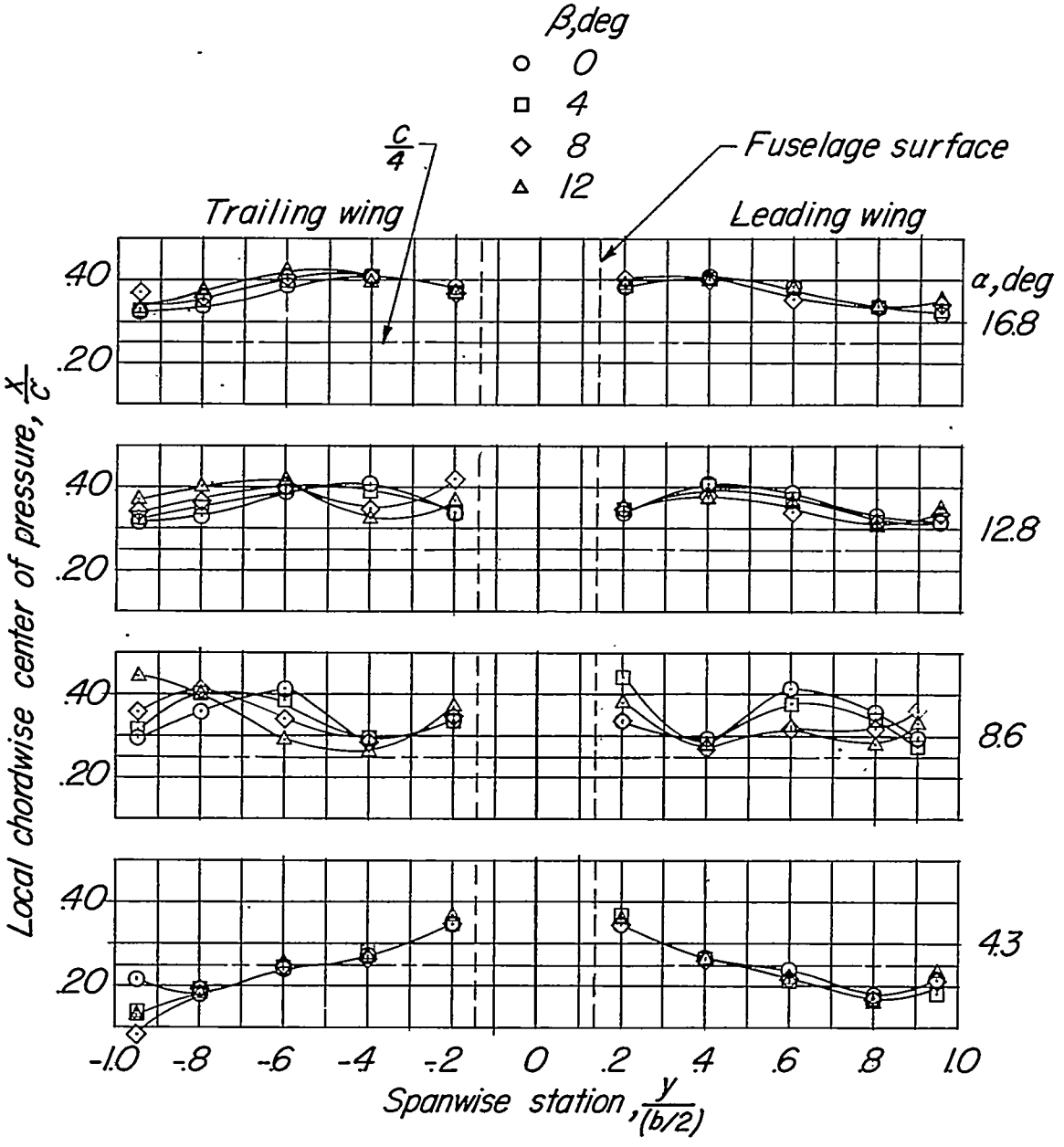

(b) M = 0.85; fence off.

Figure 5.- Continued.

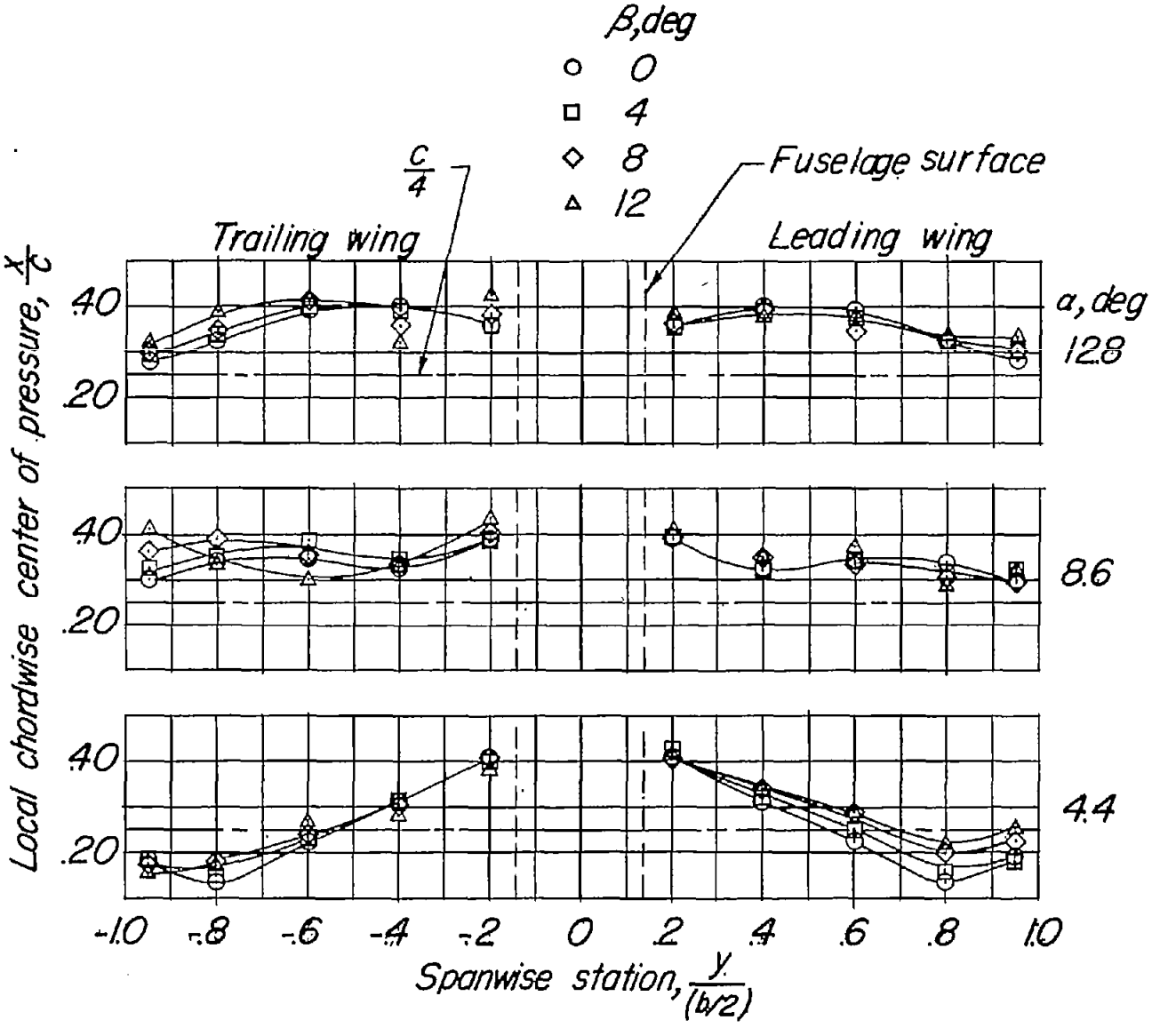

(c) M = 0.91; fence off.

Figure 5.- Continued.

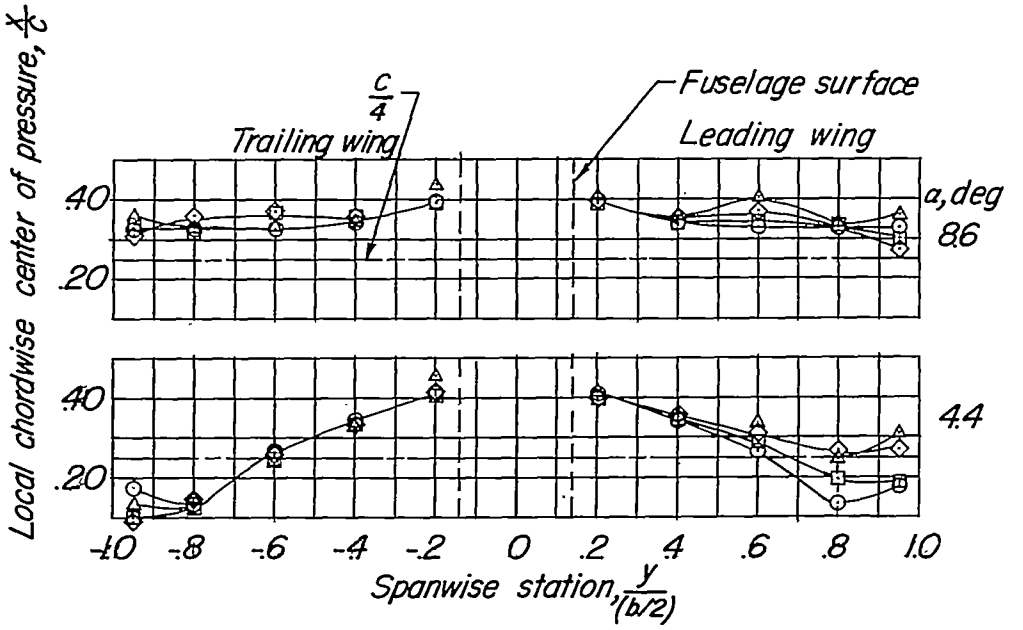

(d) M = 0.93; fence off.

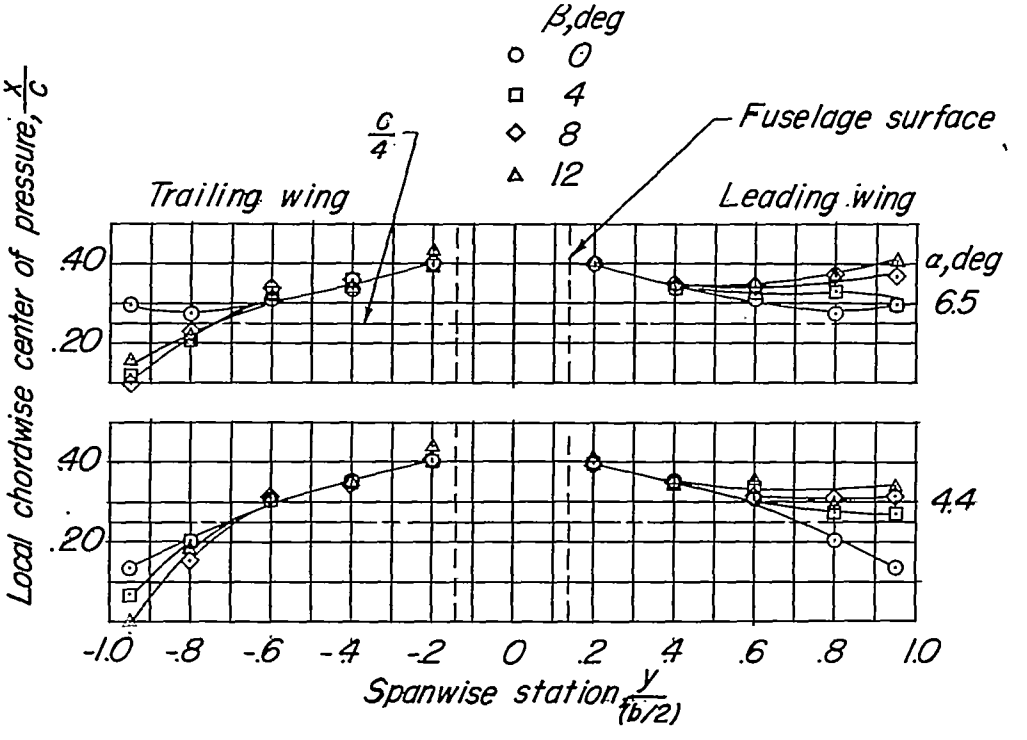

(e) M = 0.95; fence off.

Figure 5.- Concluded.

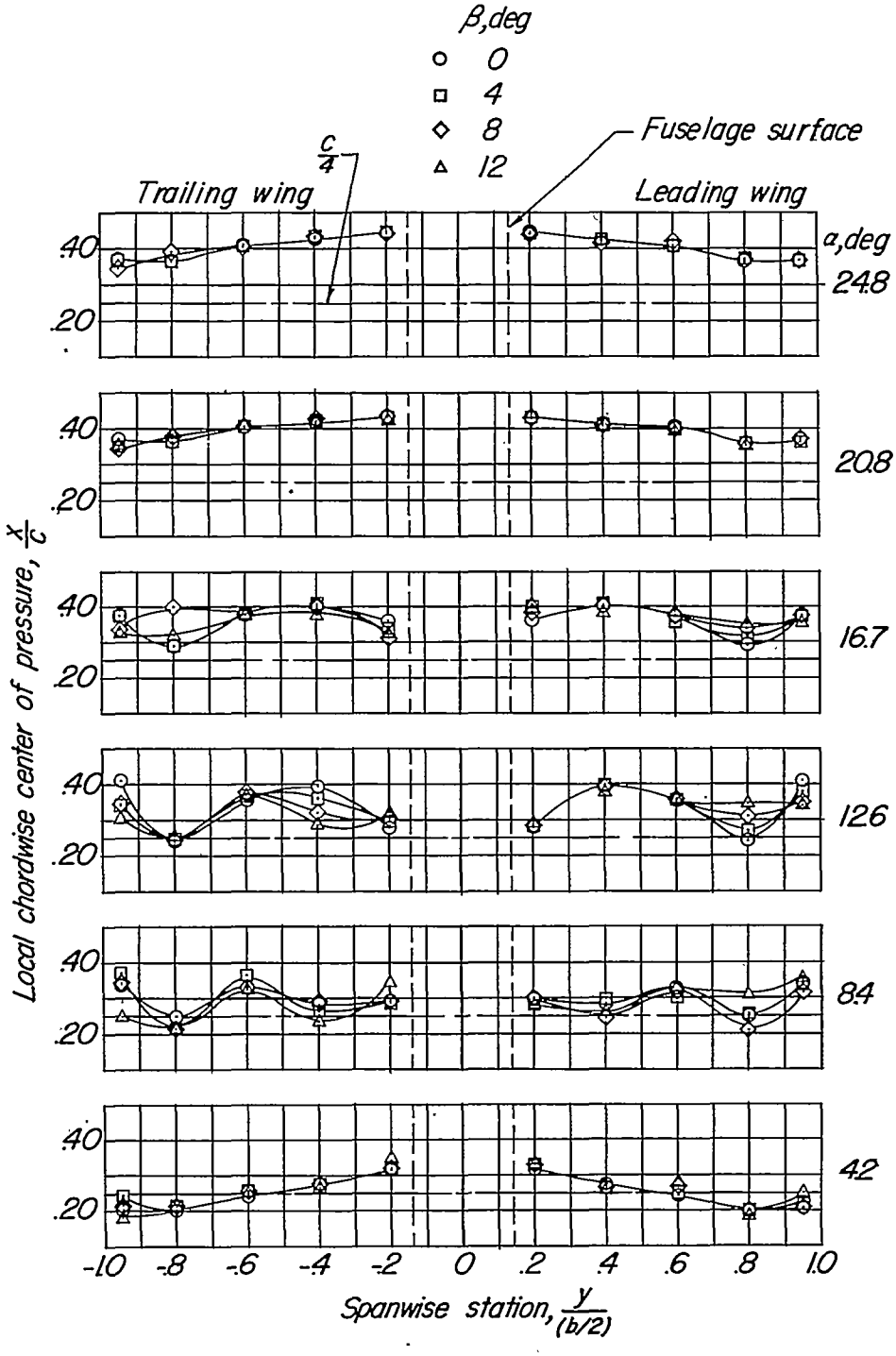

(a) M = 0.70; fence on.

Figure 6.- Effect of sideslip on location of local chordwise center of pressure with fence on.

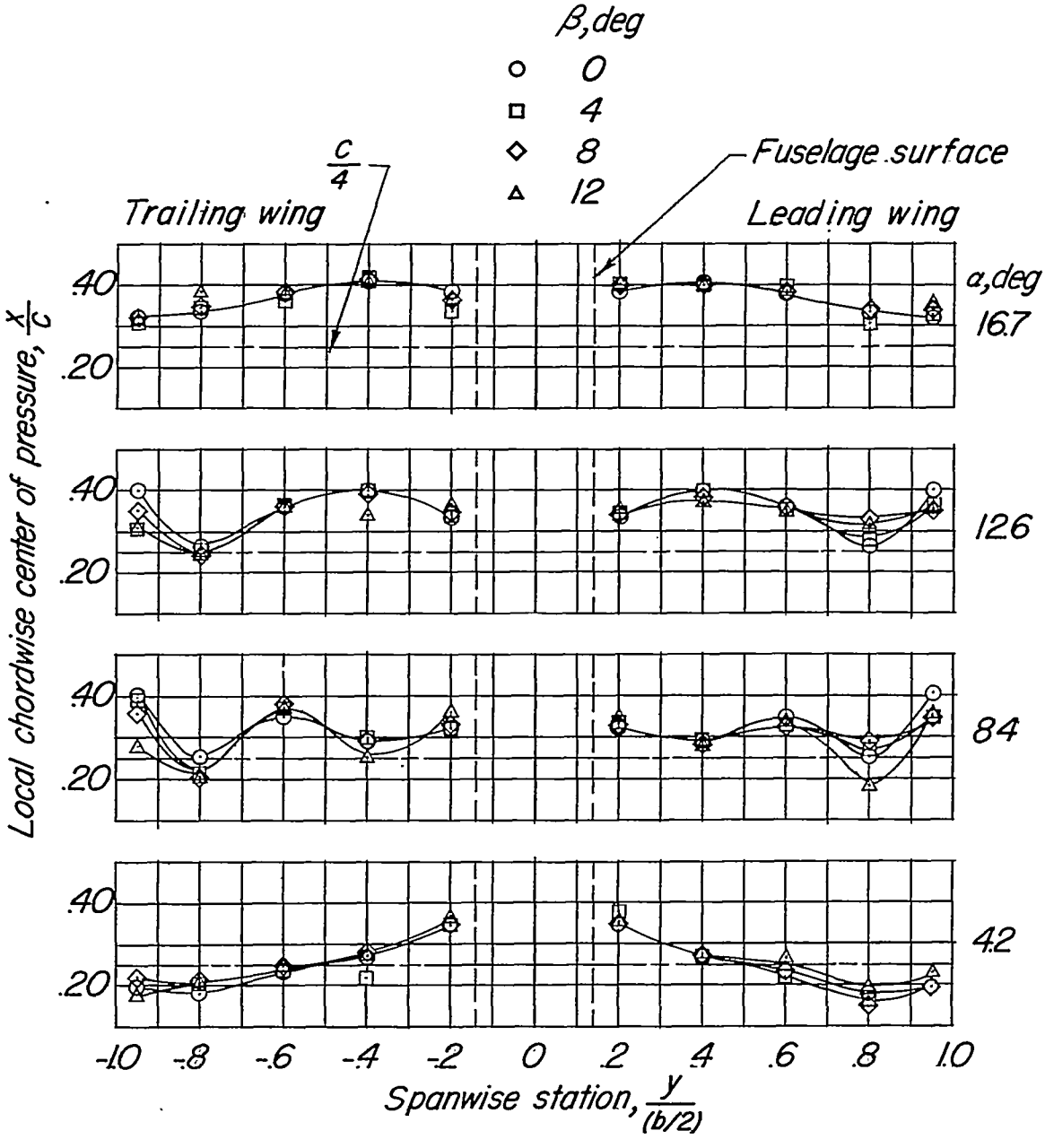

(b) M = 0.85; fence on.

Figure 6.- Continued.

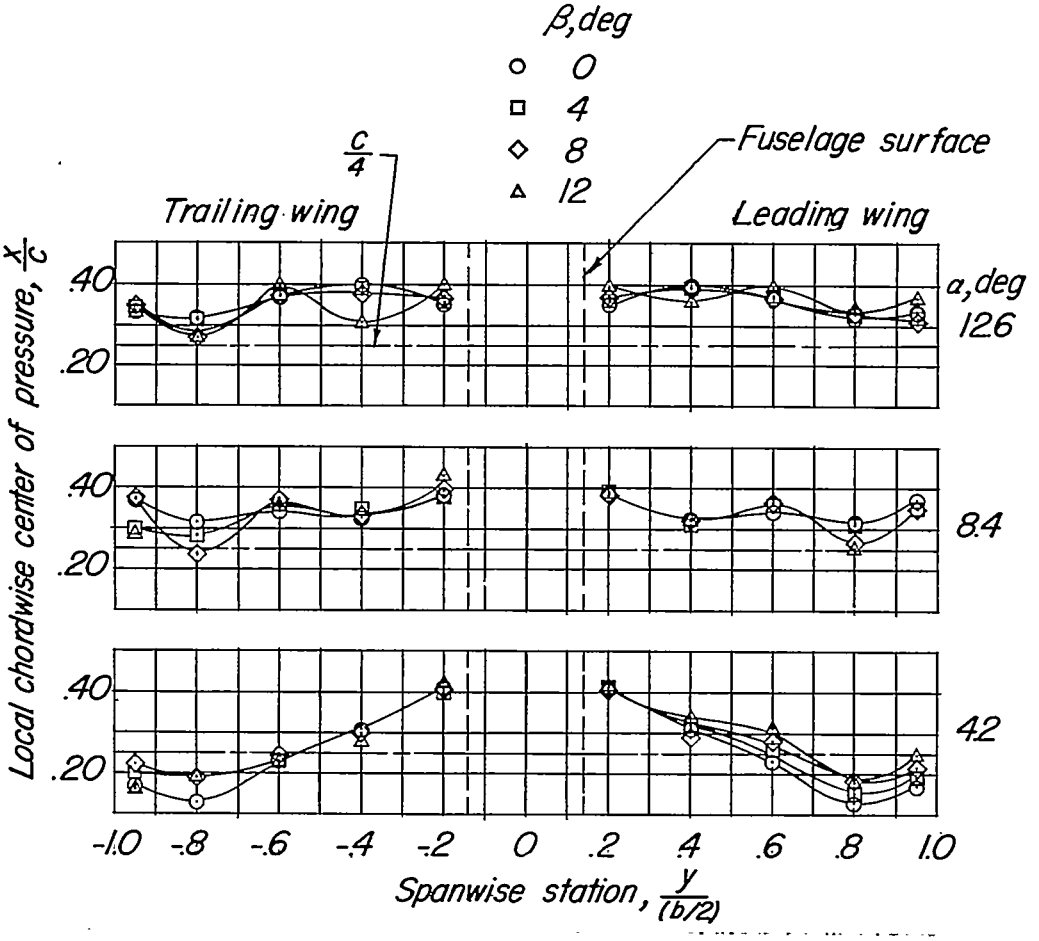

(c) M = 0.91; fence on.

Figure 6.- Continued.

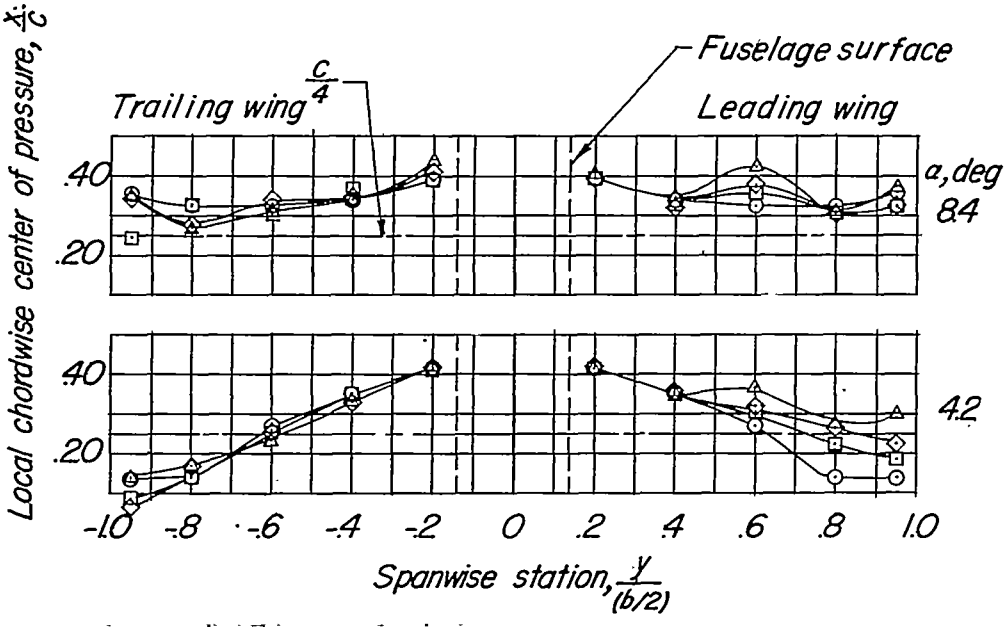

(d) M = 0.93; fence on.

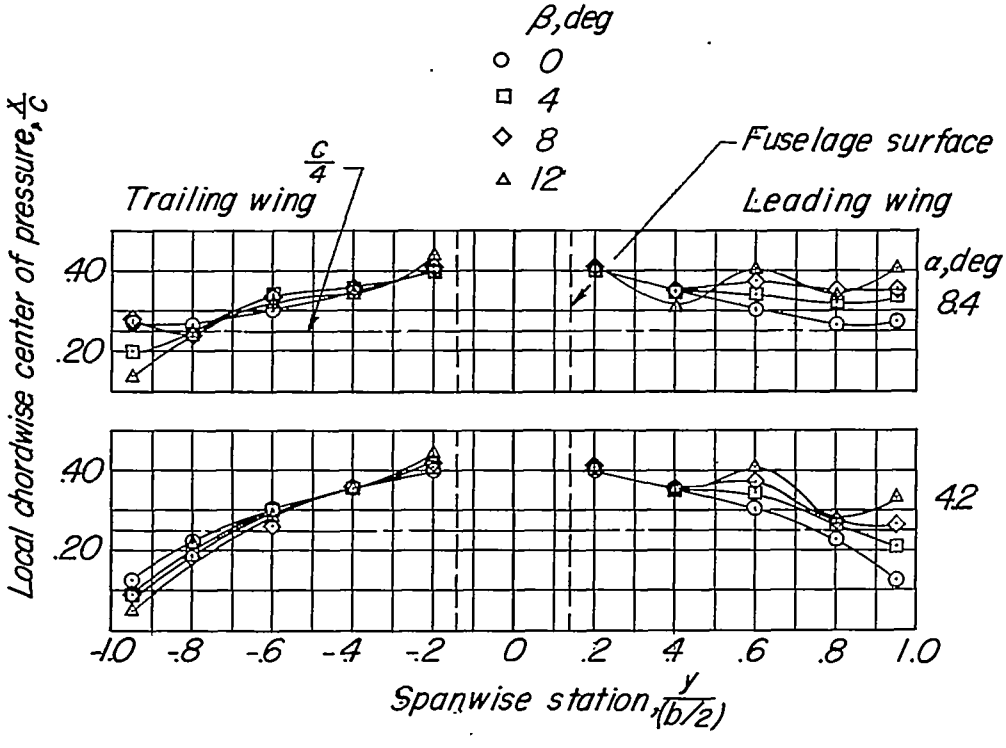

(e) M = 0.95; fence on.

Figure 6.- Concluded.

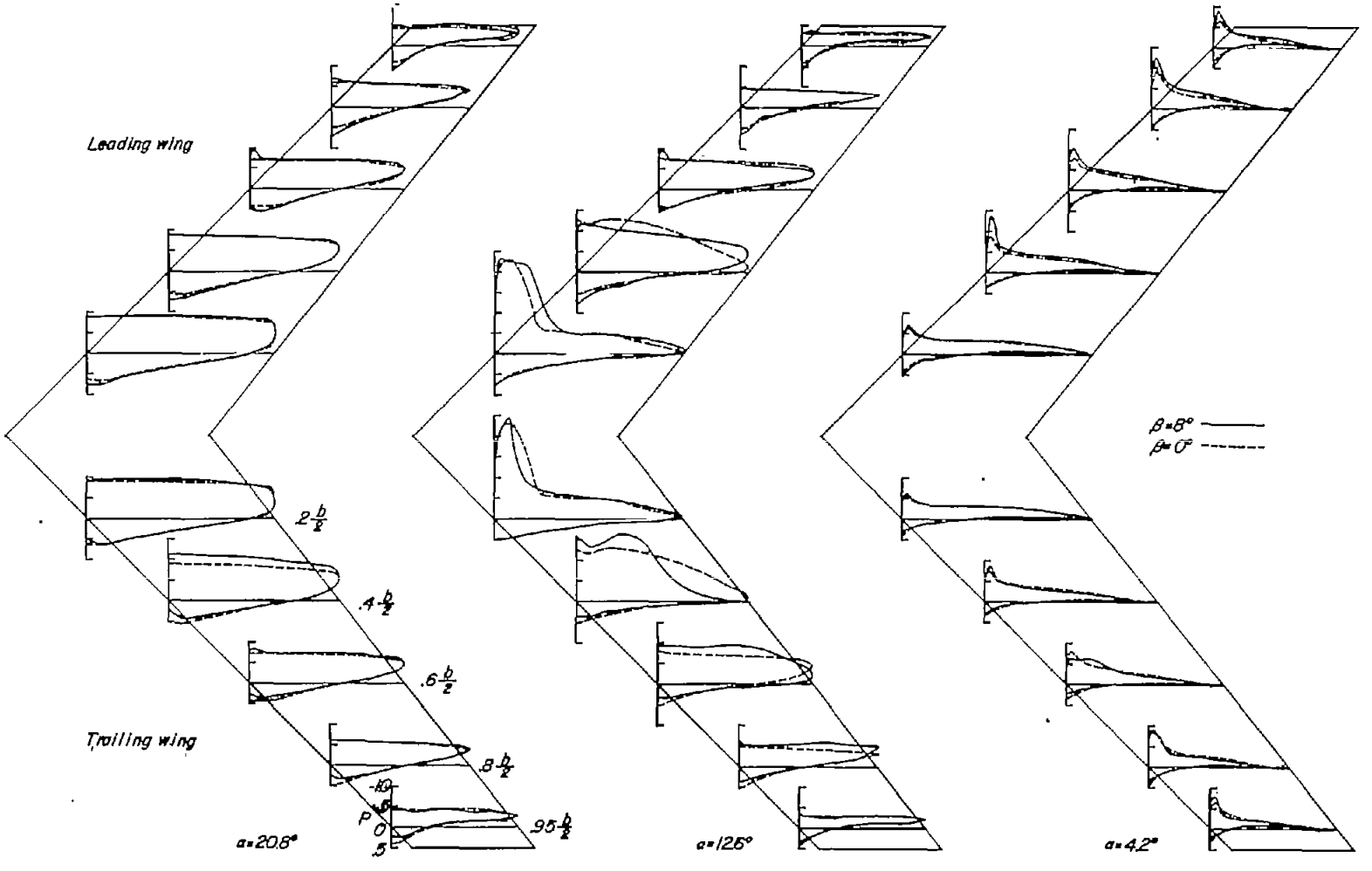

(a) M = 0.70; fence off.

Figure 7.- Effect of sideslip on chordwise load distribution.

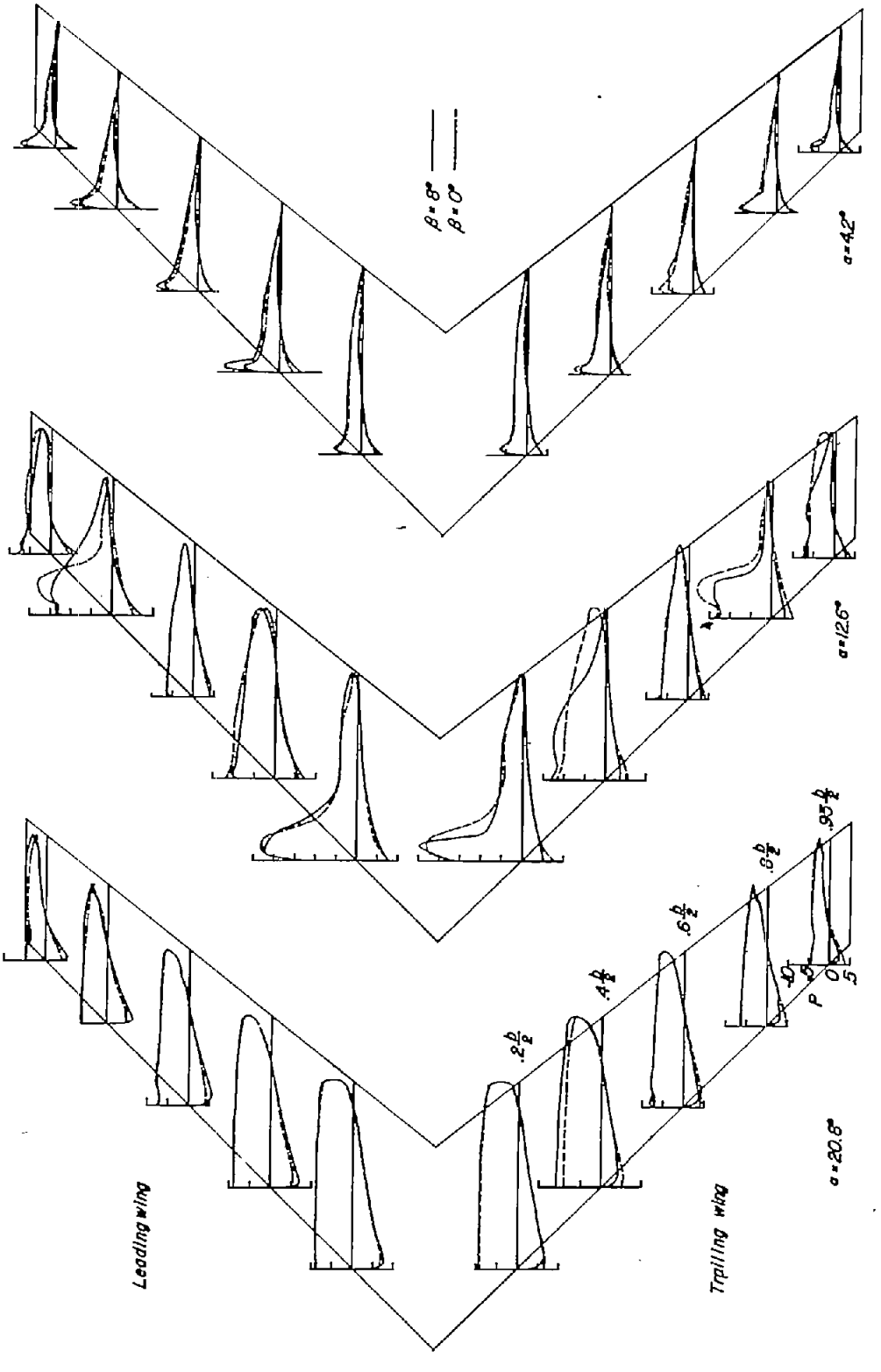

(b) M = 0.70; fence on.

Figure 7.- Continued.

[redacted]

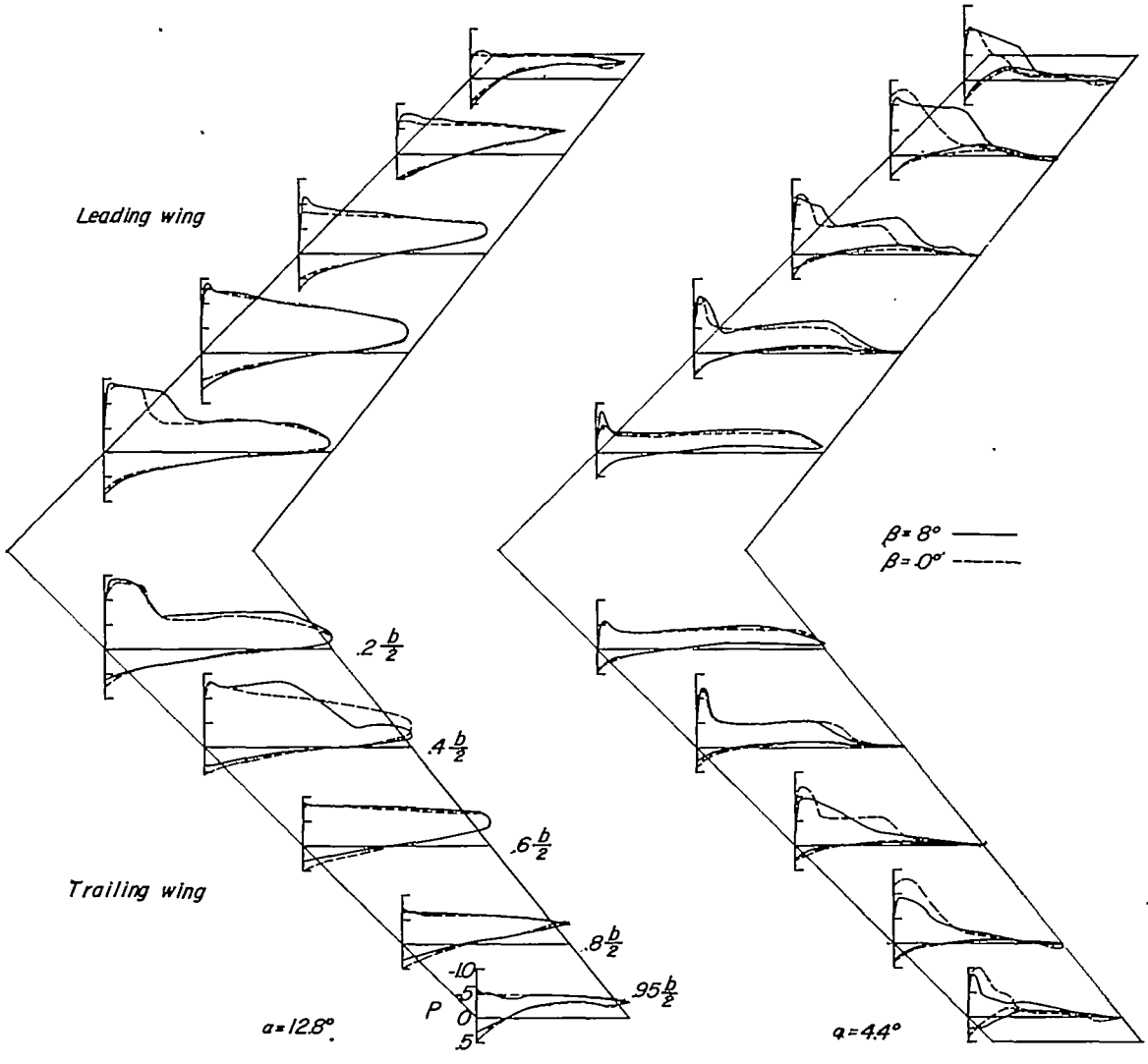

(c) M = 0.91; fence off.

Figure 7.- Continued.

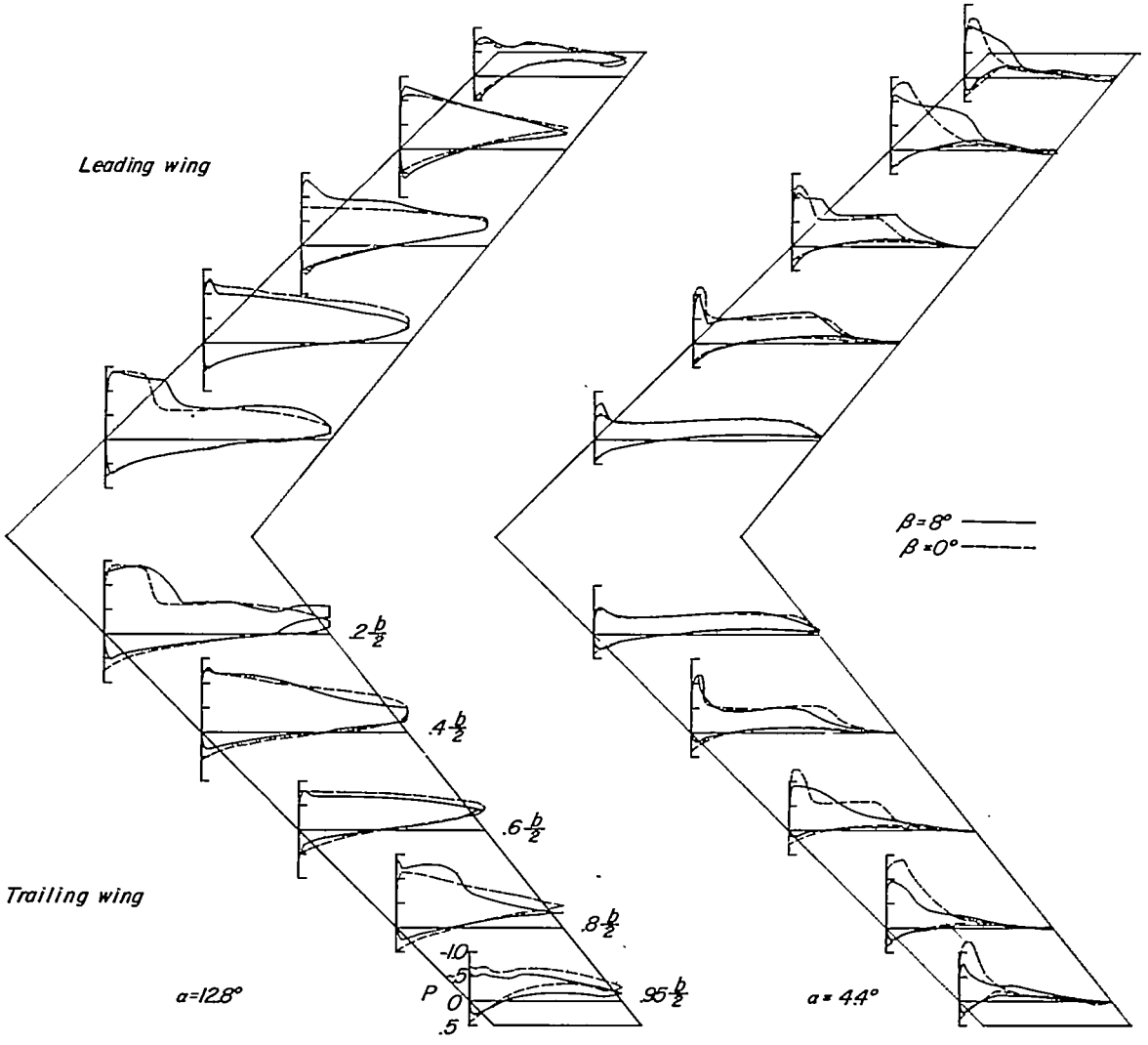

(d) M = 0.91; fence on.

Figure 7.- Concluded.

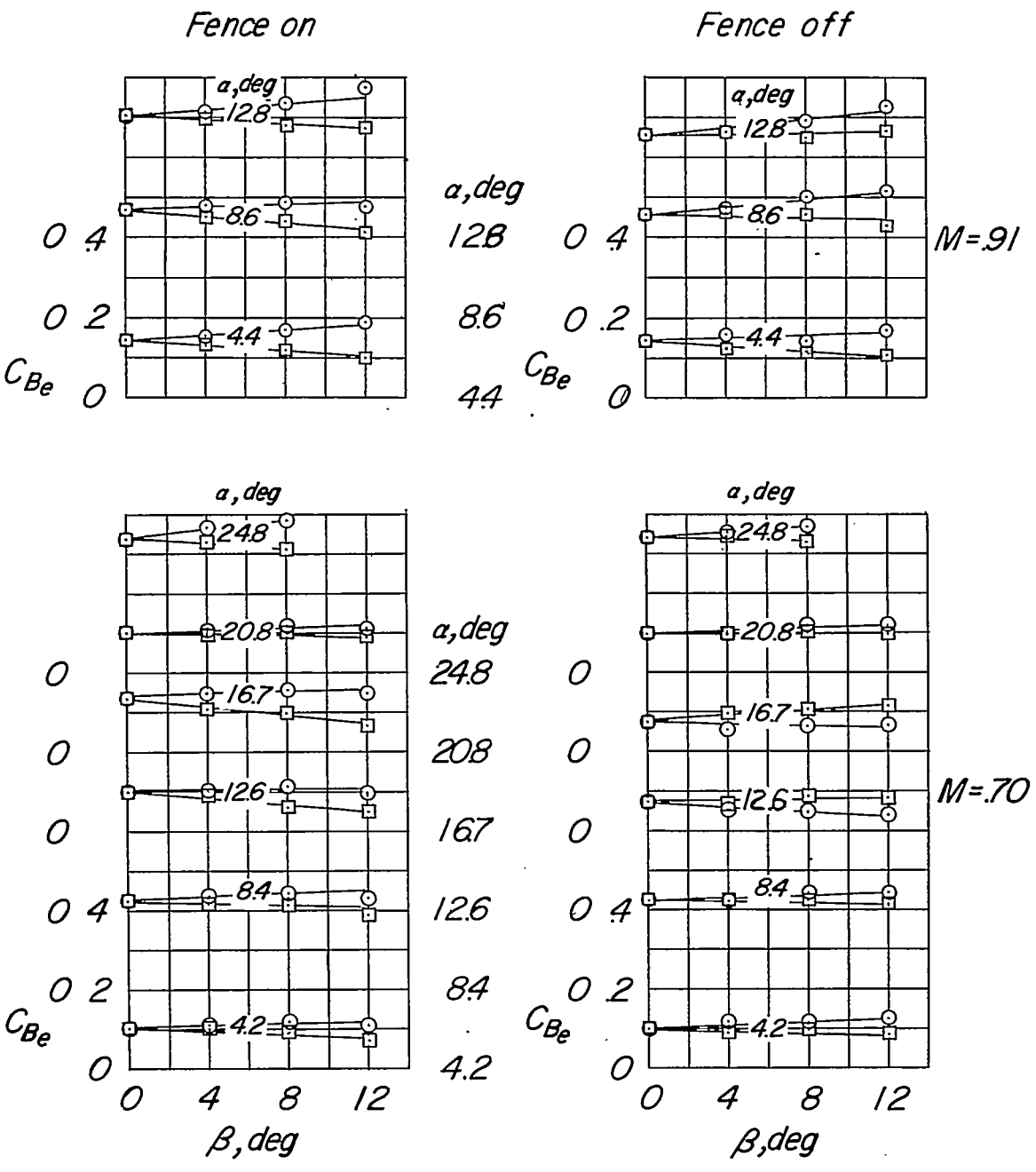

Figure 8.- Effect of sideslip on root bending-moment coefficient.

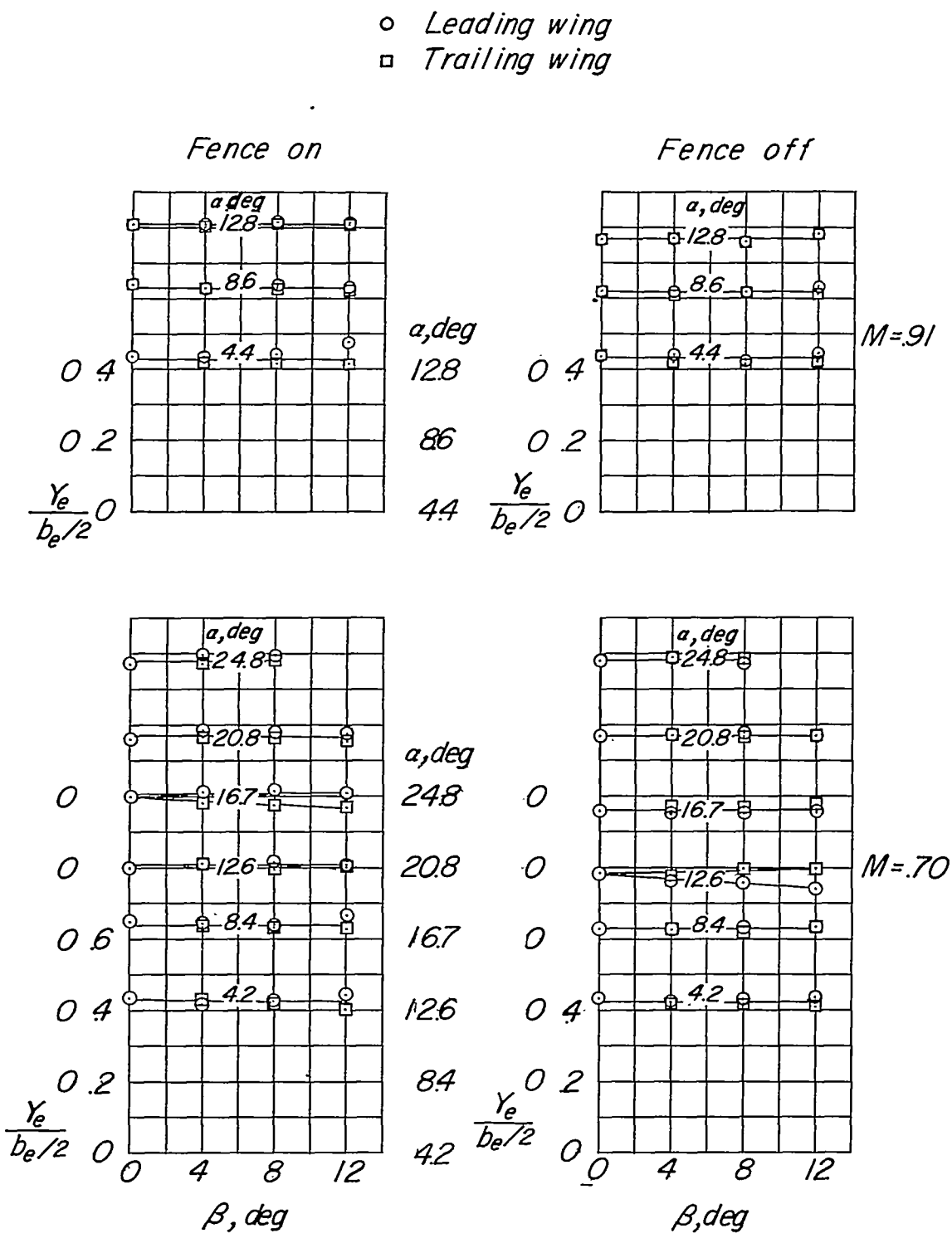

Figure 9.- Effect of sideslip on lateral center of pressure.

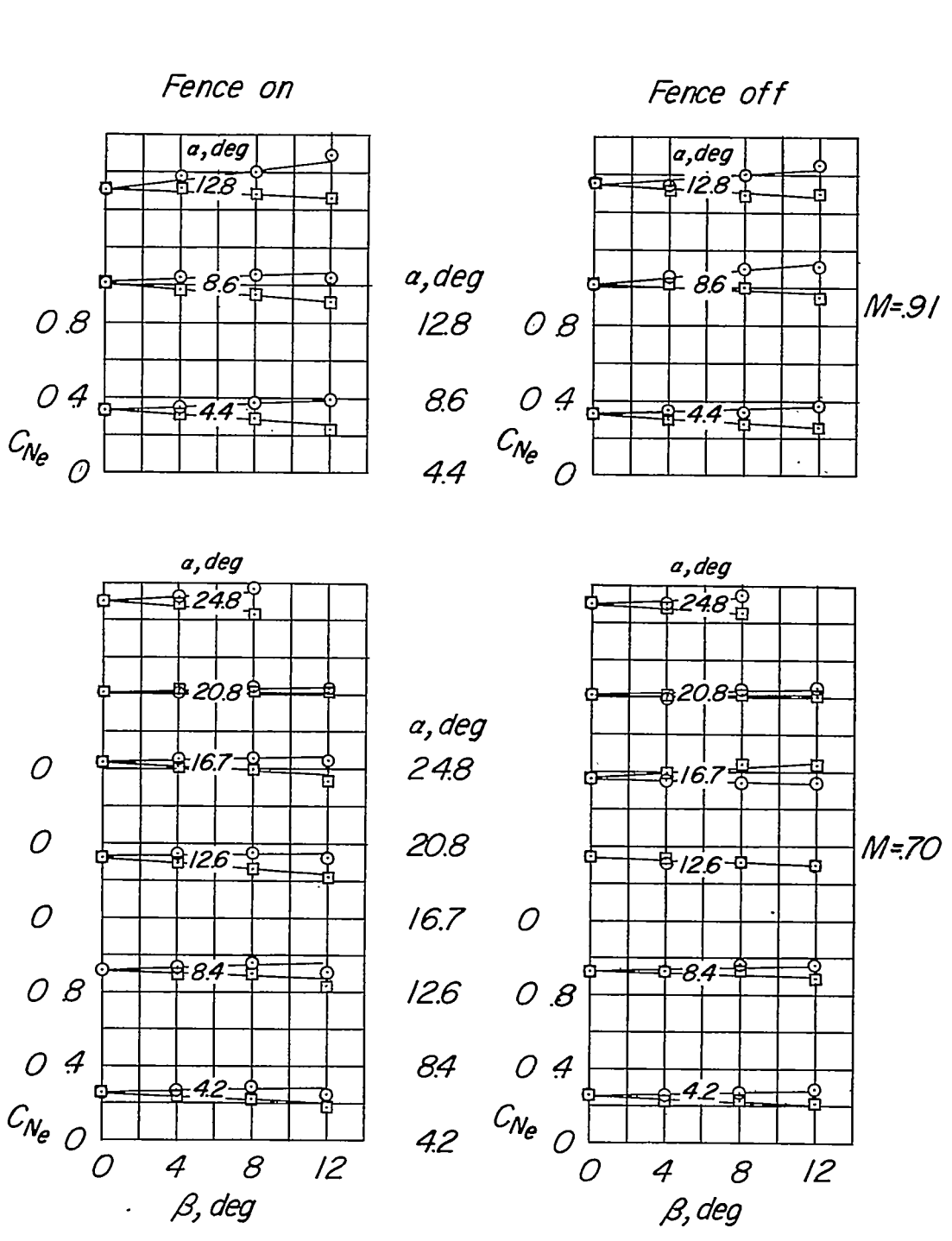

Figure 10.- Effect of sideslip on normal-force coefficient.

[redacted]

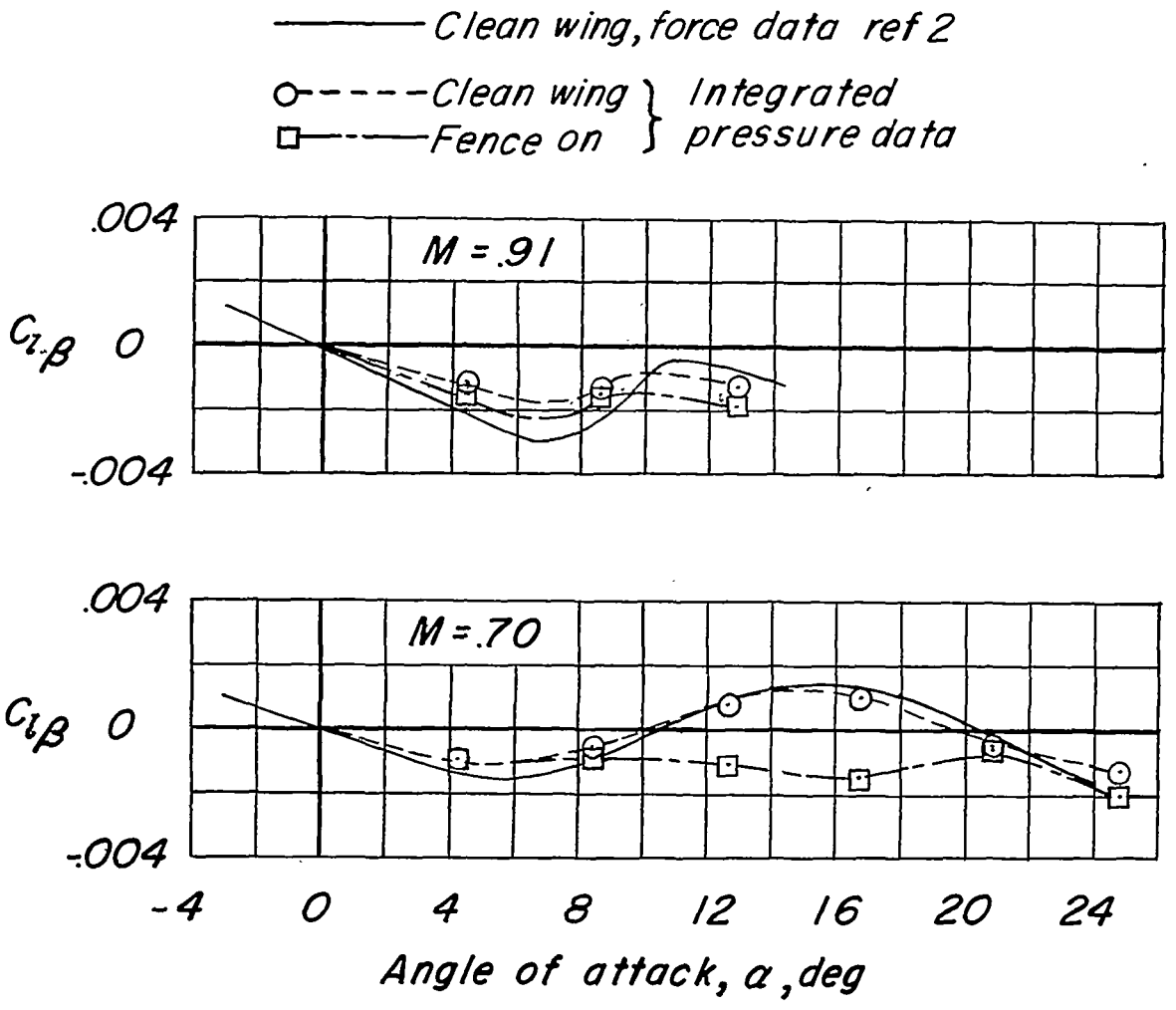

Figure 11.- Comparison of variation of rolling moment due to sideslip with angle of attack as determined from pressure distributions and force tests.

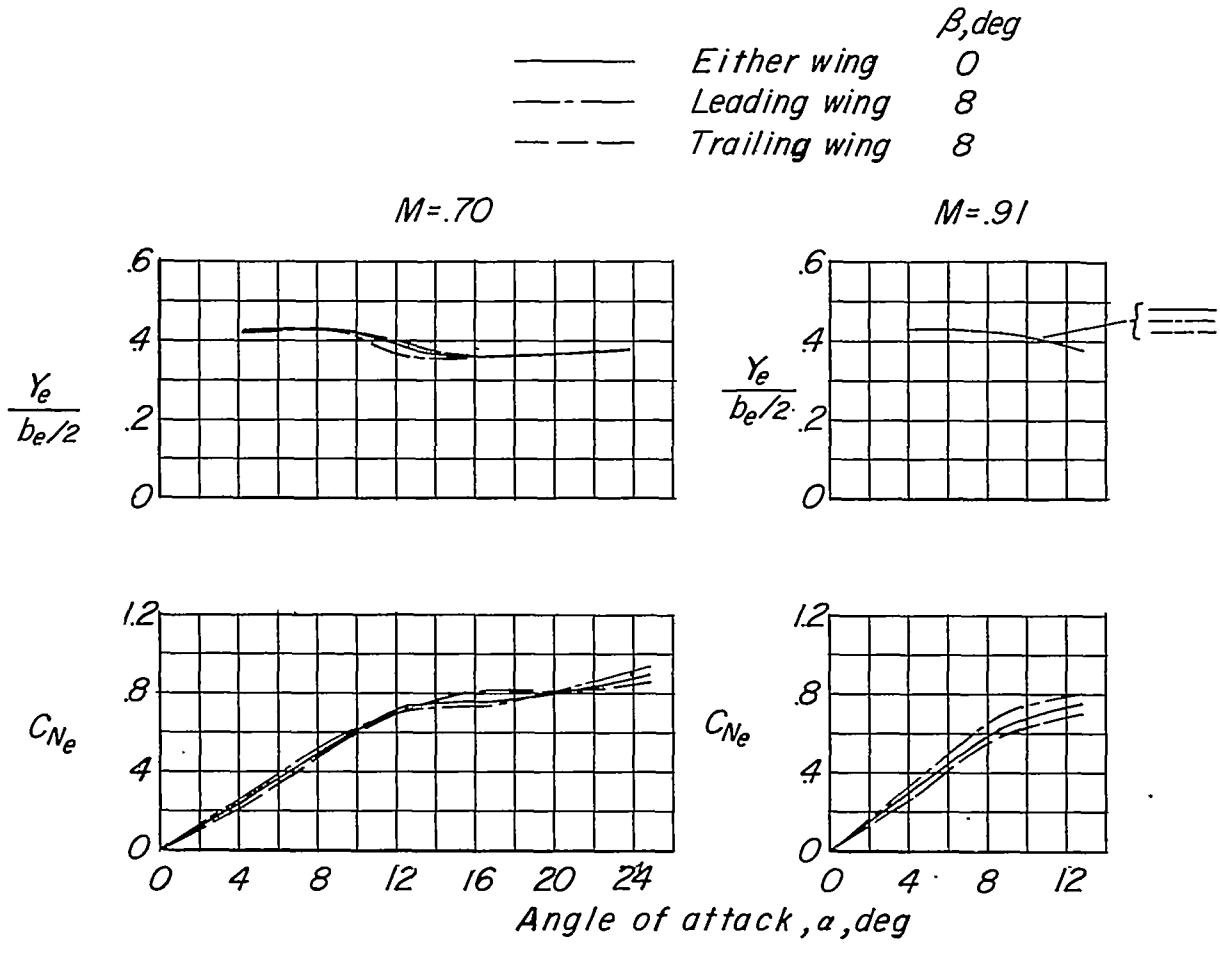

(a) Fence off.

Figure 12.- Effect of sideslip on variation of normal-force coefficient and lateral center of pressure with angle of attack.

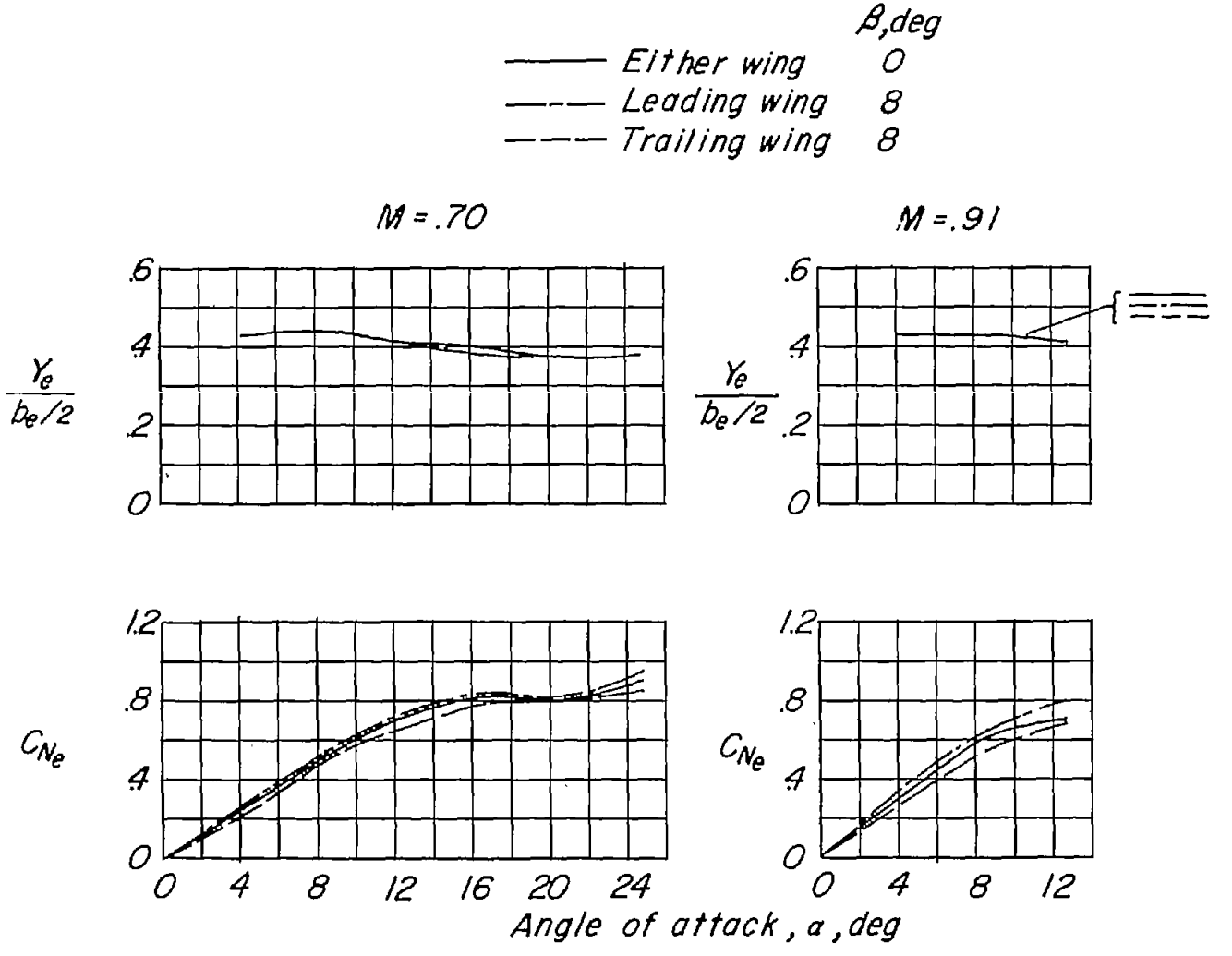

(b) Fence on.

Figure 12.- Concluded.